FERMILAB-PUB-96/098-E
MAY 8, 1996

Further Properties of High-Mass Multijet Events at the Fermilab Proton-Antiproton Collider

F. Abe,[14] H. Akimoto,[32] A. Akopian,[27] M. G. Albrow,[7] S. R. Amendolia,[23] D. Amidei,[17] J. Antos,[29] C. Anway-Wiese,[4] S. Aota,[32] G. Apollinari,[27] T. Asakawa,[32] W. Ashmanskas,[15] M. Atac,[7] F. Azfar,[22] P. Azzi-Bacchetta,[21] N. Bacchetta,[21] W. Badgett,[17] S. Bagdasarov,[27] M. W. Bailey,[19] J. Bao,[35] P. de Barbaro,[26] A. Barbaro-Galtieri,[15] V. E. Barnes,[25] B. A. Barnett,[13] E. Barzi,[8] G. Bauer,[16] T. Baumann,[9] F. Bedeschi,[23] S. Behrends,[3] S. Belforte,[23] G. Bellettini,[23] J. Bellinger,[34] D. Benjamin,[31] J. Benlloch,[16] J. Bensinger,[3] D. Benton,[22] A. Beretvas,[7] J. P. Berge,[7] J. Berryhill,[5] S. Bertolucci,[8] A. Bhatti,[27] K. Biery,[12] M. Binkley,[7] D. Bisello,[21] R. E. Blair,[1] C. Blocker,[3] A. Bodek,[26] W. Bokhari,[16] V. Bolognesi,[7] D. Bortoletto,[25] J. Boudreau,[24] L. Breccia,[2] C. Bromberg,[18] N. Bruner,[19] E. Buckley-Geer,[7] H. S. Budd,[26] K. Burkett,[17] G. Busetto,[21] A. Byon-Wagner,[7] K. L. Byrum,[1] J. Cammerata,[13] C. Campagnari,[7] M. Campbell,[17] A. Caner,[7] W. Carithers,[15] D. Carlsmith,[34] A. Castro,[21] D. Cauz,[23] Y. Cen,[26] F. Cervelli,[23] P. S. Chang,[29] P. T. Chang,[29] H. Y. Chao,[29] J. Chapman,[17] M.-T. Cheng,[29] G. Chiarelli,[23] T. Chikamatsu,[32] C. N. Chiou,[29] L. Christofek,[11] S. Cihangir,[7] A. G. Clark,[23] M. Cobal,[23] M. Contreras,[5] J. Conway,[28] J. Cooper,[7] M. Cordelli,[8] C. Couyoumtzelis,[23] D. Crane,[1] D. Cronin-Hennessy,[6] R. Culbertson,[5] J. D. Cunningham,[3] T. Daniels,[16] F. DeJongh,[7] S. Delchamps,[7] S. Dell'Agnello,[23] M. Dell'Orso,[23] R. Demina,[7] L. Demortier,[27] B. Denby,[23] M. Deninno,[2] P. F. Derwent,[17] T. Devlin,[28] J. R. Dittmann,[6] S. Donati,[23] J. Done,[30] T. Dorigo,[21] A. Dunn,[17] N. Eddy,[17]

K. Einsweiler,[15] J. E. Elias,[7] R. Ely,[15] E. Engels, Jr.,[24] D. Errede,[11] S. Errede,[11] Q. Fan,[26] I. Fiori,[2] B. Flaugher,[7] G. W. Foster,[7] M. Franklin,[9] M. Frautschi,[31] J. Freeman,[7] J. Friedman,[16] H. Frisch,[5] T. A. Fuess,[1] Y. Fukui,[14] S. Funaki,[32] G. Gagliardi,[23] S. Galeotti,[23] M. Gallinaro,[21] M. Garcia-Sciveres,[15] A. F. Garfinkel,[25] C. Gay,[9] S. Geer,[7] D. W. Gerdes,[17] P. Giannetti,[23] N. Giokaris,[27] P. Giromini,[8] L. Gladney,[22] D. Glenzinski,[13] M. Gold,[19] J. Gonzalez,[22] A. Gordon,[9] A. T. Goshaw,[6] K. Goulianos,[27] H. Grassmann,[23] L. Groer,[28] C. Grosso-Pilcher,[5] G. Guillian,[17] R. S. Guo,[29] C. Haber,[15] E. Hafen,[16] S. R. Hahn,[7] R. Hamilton,[9] R. Handler,[34] R. M. Hans,[35] K. Hara,[32] A. D. Hardman,[25] B. Harral,[22] R. M. Harris,[7] S. A. Hauger,[6] J. Hauser,[4] C. Hawk,[28] E. Hayashi,[32] J. Heinrich,[22] K. D. Hoffman,[25] M. Hohlmann,[1,5] C. Holck,[22] R. Hollebeek,[22] L. Holloway,[11] A. Hölscher,[12] S. Hong,[17] G. Houk,[22] P. Hu,[24] B. T. Huffman,[24] R. Hughes,[26] J. Huston,[18] J. Huth,[9] J. Hylen,[7] H. Ikeda,[32] M. Incagli,[23] J. Incandela,[7] G. Introzzi,[23] J. Iwai,[32] Y. Iwata,[10] H. Jensen,[7] U. Joshi,[7] R. W. Kadel,[15] E. Kajfasz,[7a] H. Kambara,[23] T. Kamon,[30] T. Kaneko,[32] K. Karr,[33] H. Kasha,[35] Y. Kato,[20] T. A. Keaffaber,[25] L. Keeble,[8] K. Kelley,[16] R. D. Kennedy,[28] R. Kephart,[7] P. Kesten,[15] D. Kestenbaum,[9] R. M. Keup,[11] H. Keutelian,[7] F. Keyvan,[4] B. Kharadia,[11] B. J. Kim,[26] D. H. Kim,[7a] H. S. Kim,[12] S. B. Kim,[17] S. H. Kim,[32] Y. K. Kim,[15] L. Kirsch,[3] P. Koehn,[26] K. Kondo,[32] J. Konigsberg,[9] S. Kopp,[5] K. Kordas,[12] A. Korytov,[16] W. Koska,[7] E. Kovacs,[7a] W. Kowald,[6] M. Krasberg,[17] J. Kroll,[7] M. Kruse,[25] T. Kuwabara,[32] S. E. Kuhlmann,[1] E. Kuns,[28] A. T. Laasanen,[25] N. Labanca,[23] S. Lammel,[7] J. I. Lamoureux,[3] T. LeCompte,[1] S. Leone,[23] J. D. Lewis,[7] P. Limon,[7] M. Lindgren,[4] T. M. Liss,[11] N. Lockyer,[22] O. Long,[22] C. Loomis,[28] M. Loreti,[21] J. Lu,[30] D. Lucchesi,[23] P. Lukens,[7] S. Lusin,[34] J. Lys,[15] K. Maeshima,[7] A. Maghakian,[27] P. Maksimovic,[16] M. Mangano,[23] J. Mansour,[18] M. Mariotti,[21] J. P. Marriner,[7] A. Martin,[11] J. A. J. Matthews,[19] R. Mattingly,[16] P. McIntyre,[30] P. Melese,[27] A. Menzione,[23] E. Meschi,[23] S. Metzler,[22] C. Miao,[17] T. Miao,[7] G. Michail,[9] R. Miller,[18] H. Minato,[32] S. Miscetti,[8] M. Mishina,[14] H. Mitsushio,[32] T. Miyamoto,[32]

S. Miyashita,[32] N. Moggi,[23] Y. Morita,[14] J. Mueller,[24] A. Mukherjee,[7] T. Muller,[4] P. Murat,[23] H. Nakada,[32] I. Nakano,[32] C. Nelson,[7] D. Neuberger,[4] C. Newman-Holmes,[7] M. Ninomiya,[32] L. Nodulman,[1] S. H. Oh,[6] K. E. Ohl,[35] T. Ohmoto,[10] T. Ohsugi,[10] R. Oishi,[32] M. Okabe,[32] T. Okusawa,[20] R. Oliveira,[22] J. Olsen,[34] C. Pagliarone,[2] R. Paoletti,[23] V. Papadimitriou,[31] S. P. Pappas,[35] S. Park,[7] A. Parri,[8] J. Patrick,[7] G. Pauletta,[23] M. Paulini,[15] A. Perazzo,[23] L. Pescara,[21] M. D. Peters,[15] T. J. Phillips,[6] G. Piacentino,[2] M. Pillai,[26] K. T. Pitts,[7] R. Plunkett,[7] L. Pondrom,[34] J. Proudfoot,[1] F. Ptohos,[9] G. Punzi,[23] K. Ragan,[12] A. Ribon,[21] F. Rimondi,[2] L. Ristori,[23] W. J. Robertson,[6] T. Rodrigo,[7a] S. Rolli,[23] J. Romano,[5] L. Rosenson,[16] R. Roser,[11] W. K. Sakumoto,[26] D. Saltzberg,[5] A. Sansoni,[8] L. Santi,[23] H. Sato,[32] V. Scarpine,[30] P. Schlabach,[9] E. E. Schmidt,[7] M. P. Schmidt,[35] A. Scribano,[23] S. Segler,[7] S. Seidel,[19] Y. Seiya,[32] G. Sganos,[12] M. D. Shapiro,[15] N. M. Shaw,[25] Q. Shen,[25] P. F. Shepard,[24] M. Shimojima,[32] M. Shochet,[5] J. Siegrist,[15] A. Sill,[31] P. Sinervo,[12] P. Singh,[24] J. Skarha,[13] K. Sliwa,[33] F. D. Snider,[13] T. Song,[17] J. Spalding,[7] T. Speer,[23] P. Sphicas,[16] F. Spinella,[23] M. Spiropulu,[9] L. Spiegel,[7] L. Stanco,[21] J. Steele,[34] A. Stefanini,[23] K. Strahl,[12] J. Strait,[7] R. Ströhmer,[9] D. Stuart,[7] G. Sullivan,[5] A. Soumarokov,[29] K. Sumorok,[16] J. Suzuki,[32] T. Takada,[32] T. Takahashi,[20] T. Takano,[32] K. Takikawa,[32] N. Tamura,[10] F. Tartarelli,[23] W. Taylor,[12] P. K. Teng,[29] Y. Teramoto,[20] S. Tether,[16] D. Theriot,[7] T. L. Thomas,[19] R. Thun,[17] M. Timko,[33] P. Tipton,[26] A. Titov,[27] S. Tkaczyk,[7] D. Toback,[5] K. Tollefson,[26] A. Tollestrup,[7] J. Tonnison,[25] J. F. de Troconiz,[9] S. Truitt,[17] J. Tseng,[13] N. Turini,[23] T. Uchida,[32] N. Uemura,[32] F. Ukegawa,[22] G. Unal,[22] J. Valls,[7] S. C. van den Brink,[24] S. Vejcik, III,[17] G. Velev,[23] R. Vidal,[7] M. Vondracek,[11] D. Vucinic,[16] R. G. Wagner,[1] R. L. Wagner,[7] J. Wahl,[5] C. Wang,[6] C. H. Wang,[29] G. Wang,[23] J. Wang,[5] M. J. Wang,[29] Q. F. Wang,[27] A. Warburton,[12] T. Watts,[28] R. Webb,[30] C. Wei,[6] C. Wendt,[34] H. Wenzel,[15] W. C. Wester, III,[7] A. B. Wicklund,[1] E. Wicklund,[7] R. Wilkinson,[22] H. H. Williams,[22] P. Wilson,[5] B. L. Winer,[26] D. Wolinski,[17] J. Wolinski,[18] X. Wu,[23] J. Wyss,[21] A. Yagil,[7]

W. Yao,[15] K. Yasuoka,[32] Y. Ye,[12] G. P. Yeh,[7] P. Yeh,[29] M. Yin,[6] J. Yoh,[7] C. Yosef,[18] T. Yoshida,[20] D. Yovanovitch,[7] I. Yu,[35] L. Yu,[19] J. C. Yun,[7] A. Zanetti,[23] F. Zetti,[23] L. Zhang,[34] W. Zhang,[22] and S. Zucchelli[2]

(CDF Collaboration)

[1] *Argonne National Laboratory, Argonne, Illinois 60439*

[2] *Istituto Nazionale di Fisica Nucleare, University of Bologna, I-40126 Bologna, Italy*

[3] *Brandeis University, Waltham, Massachusetts 02254*

[4] *University of California at Los Angeles, Los Angeles, California 90024*

[5] *University of Chicago, Chicago, Illinois 60637*

[6] *Duke University, Durham, North Carolina 27708*

[7] *Fermi National Accelerator Laboratory, Batavia, Illinois 60510*

[8] *Laboratori Nazionali di Frascati, Istituto Nazionale di Fisica Nucleare, I-00044 Frascati, Italy*

[9] *Harvard University, Cambridge, Massachusetts 02138*

[10] *Hiroshima University, Higashi-Hiroshima 724, Japan*

[11] *University of Illinois, Urbana, Illinois 61801*

[12] *Institute of Particle Physics, McGill University, Montreal H3A 2T8, and University of Toronto, Toronto M5S 1A7, Canada*

[13] *The Johns Hopkins University, Baltimore, Maryland 21218*

[14] *National Laboratory for High Energy Physics (KEK), Tsukuba, Ibaraki 305, Japan*

[15] *Ernest Orland Lawrence Berkeley Laboratory, Berkeley, California 94720*

[16] *Massachusetts Institute of Technology, Cambridge, Massachusetts 02139*

[17] *University of Michigan, Ann Arbor, Michigan 48109*

[18] *Michigan State University, East Lansing, Michigan 48824*

[19] *University of New Mexico, Albuquerque, New Mexico 87131*

[20] *Osaka City University, Osaka 588, Japan*

[21] *Universita di Padova, Istituto Nazionale di Fisica Nucleare, Sezione di Padova, I-35131 Padova, Italy*

[22] University of Pennsylvania, Philadelphia, Pennsylvania 19104

[23] Istituto Nazionale di Fisica Nucleare, University and Scuola Normale Superiore of Pisa, I-56100 Pisa, Italy

[24] University of Pittsburgh, Pittsburgh, Pennsylvania 15260

[25] Purdue University, West Lafayette, Indiana 47907

[26] University of Rochester, Rochester, New York 14627

[27] Rockefeller University, New York, New York 10021

[28] Rutgers University, Piscataway, New Jersey 08854

[29] Academia Sinica, Taipei, Taiwan 11529, Republic of China

[30] Texas A&M University, College Station, Texas 77843

[31] Texas Tech University, Lubbock, Texas 79409

[32] University of Tsukuba, Tsukuba, Ibaraki 305, Japan

[33] Tufts University, Medford, Massachusetts 02155

[34] University of Wisconsin, Madison, Wisconsin 53706

[35] Yale University, New Haven, Connecticut 06511

PACS numbers: 12.38Qk, 13.85.-t, 13.85.Hd, 13.87.-a

Abstract

The properties of high-mass multijet events produced at the Fermilab proton-antiproton collider are compared with leading order QCD matrix element predictions, QCD parton shower Monte Carlo predictions, and the predictions from a model in which events are distributed uniformly over the available multibody phase-space. Multijet distributions corresponding to (4N-4) variables that span the N-body parameter space are found to be well described by the QCD calculations for inclusive three-jet, four-jet, and five-jet

events. The agreement between data, QCD Matrix Element calculations, and QCD parton shower Monte Carlo predictions suggests that $2 \rightarrow 2$ scattering plus gluon radiation provides a good first approximation to the full LO QCD matrix element for events with three, four, or even five jets in the final state.

1 Introduction

A study of the properties of events containing three-or-more jets produced in high-energy hadron-hadron collisions can (i) test our understanding of the higher-order QCD processes that result in multijet production, (ii) test the QCD parton shower Monte Carlo approximation to the full leading order (LO) QCD matrix element, and (iii) enable a search for new phenomena associated with the presence of many hard partons in the final state. The CDF collaboration has recently reported the characteristics of two-jet, three-jet, four-jet, five-jet, and six-jet events [1] produced at the Tevatron proton-antiproton collider operating at a center-of-mass energy of 1.8 TeV. Results from an analysis of events with multijet masses exceeding 600 GeV/c^2 were presented for a data sample corresponding to an integrated luminosity of 35 pb^{-1}. The multijet-mass distributions, leading-jet angular distributions, and mass dependent jet multiplicity distributions were shown to be well described by both the NJETS [2] LO QCD matrix element calculation for events with up to five jets, and the HERWIG [3] QCD parton shower Monte Carlo calculation for events with up to six jets. For these selected distributions the QCD predictions were found to give a good description of the data.

In the present paper we use a larger data sample and a more comprehensive set of multijet distributions to extend our comparison of the properties of high-mass multijet events with QCD predictions. In particular, we use the set of (4N-4) variables that span the N-jet parameter space and were recently proposed by Geer and Asakawa [4], and compare the observed three-jet, four-jet, and five-jet event characteristics with (a)

NJETS LO QCD matrix element predictions, (b) HERWIG parton shower Monte Carlo predictions, and (c) predictions from a model in which events are uniformly distributed over the available multijet phase-space. Results are based on a data sample which was recorded by the CDF collaboration during the period 1992 - 1995, and corresponds to an integrated luminosity of 105 pb^{-1}.

2 Experimental Details

A description of the CDF detector can be found in Ref. [5]. Full details of the CDF jet algorithm, jet corrections, and jet resolution functions can be found in Ref. [6], and a description of the trigger and event selection requirements for the high-mass multijet sample are given in Ref. [1]. In the following we give a summary of the main details of the CDF detector, jet reconstruction, and event selection requirements that are relevant to results presented in this paper. We use the CDF co-ordinate system in which the origin is at the center of the detector, the z-axis is along the beam direction, θ is the polar angle with respect to the z-axis, and ϕ is the azimuthal angle measured around the beam direction.

The multijet analysis described in the following sections exploits the CDF calorimeters, which cover the pseudorapidity region $|\eta| < 4.2$, where $\eta \equiv -\ln(\tan\theta/2)$. The calorimeters are constructed in a tower geometry in η - ϕ space, and are segmented in depth into electromagnetic and hadronic compartments. The calorimeter towers are 0.1 units wide in η. The tower widths in ϕ are 15^o in the central region and 5^o at larger

$|\eta|$ (approximately $|\eta| > 1.2$). Jets are reconstructed using an algorithm that forms clusters from localized energy depositions in the calorimeter towers. Calorimeter towers are associated with a jet if their separation from the jet axis in (η, ϕ)-space $\Delta\mathrm{R} = (\Delta\eta^2 + \Delta\phi^2)^{1/2} < R_0$. For the analysis described in this paper the clustering cone radius $R_0 = 0.7$ was chosen. With this R_0 a plot of the separation between all jets observed in the data sample described below reveals that, to a good approximation, clusters with separations $\Delta R < 0.8$ are always merged by the jet algorithm into a single jet, and clusters with separations $\Delta R > 1.0$ are never merged. Thus, the effective minimum observable separation between jets $\Delta R_{MIN} = 0.9 \pm 0.1$. Jet energies are corrected for calorimeter non-linearities, energy lost in uninstrumented regions and outside of the clustering cone, and energy gained from the underlying event. The jet corrections typically increase jet energies by 25% for jets with transverse energy $E_T = E \sin\theta >$ 60 GeV, where θ is the angle between the jet axis and the beam direction. The jet corrections are larger for lower E_T jets, and typically increase jet energies by about 30% (40%) for jets with $E_T = 40$ GeV (20 GeV). After correction, jet energies are measured with a precision σ_E/E of approximately 0.1 and multijet masses calculated from the jet four-vectors are measured with a precision σ_m/m of approximately 0.1. The systematic uncertainty on the jet energy scale is 5% for jets in the central region ($|\eta| < 1.2$). There is an additional systematic uncertainty of 2% on the energy scale of jets at larger $|\eta|$ relative to the corresponding scale for central jets.

The data were recorded using a trigger which required $\sum E_T > 300$ GeV, where the sum is over the transverse energies (E_T) of all uncorrected jets with $E_T > 10$ GeV, and the jet transverse energies were calculated assuming an event vertex at the center of the detector (x=y=z=0). In the subsequent analysis the $\sum E_T$ was recalculated using the reconstructed vertex position and corrected jet energies, and summing over all jets with corrected $E_T > 20$ GeV. Events were retained with $\sum E_T > 420$ GeV. To reject backgrounds from cosmic ray interactions, beam halo, and detector malfunctions, the events were required to have (i) total energy less than 2000 GeV, (ii) a primary vertex reconstructed with $|z| < 60$ cm, (iii) no significant energy deposited in the hadron calorimeters out-of-time with the proton-antiproton collision, and (iv) missing-E_T significance [7] $S \equiv \not{E}_T \, / (\sum E_T \,)^{1/2} < 6$, where $\not{E}_T \, \equiv |\sum \overline{E_T}_i|$, and $\overline{E_T}_i$ is a vector that points from the interaction vertex to calorimeter cell i and has magnitude equal to the cell E_T. These requirements select 30245 events.

3 QCD and Phase-Space Predictions

In the following we will compare observed multijet distributions with predictions from (a) the HERWIG [3] QCD parton shower Monte Carlo program, (b) the NJETS [2] LO QCD $2 \to N$ matrix element Monte Carlo program, and (c) a model in which events are distributed uniformly over the available N-body phase-space.

3.1 The HERWIG Parton Shower Monte Carlo Calculation

HERWIG [3] is a QCD parton shower Monte Carlo program that includes both initial- and final-state gluon radiation. HERWIG predictions can be thought of as QCD $2 \rightarrow 2$ predictions with gluon radiation, color coherence, hadronization, and an underlying event. We have used version 5.6 of the HERWIG Monte Carlo program together with a full simulation of the CDF detector response. In our HERWIG calculations we have used the CTEQ1M [8] structure functions and the scale $\mathrm{Q}^2 = \mathrm{stu}/2(\mathrm{s}^2+\mathrm{u}^2+\mathrm{t}^2)$. HERWIG generates $2 \rightarrow 2$ processes above a specified p_T^{hard} where p_T^{hard} is the p_T of the outgoing partons from the hard scatter before any radiation has occurred. It is important to chose a low value of p_T^{hard} so that adequate account is taken of events in which the detector response has fluctuated upwards by several standard deviations and/or the spectator system accompanying the hard scattering process, including the initial state radiation, makes an unusually large contribution to the $\sum E_T$. We have set the minimum p_T^{hard} to 60 GeV/c. The contribution to the $\sum E_T > 420$ GeV Monte Carlo sample from events with $p_T^{hard} < 60$ GeV/c is estimated to be less than 1%.

3.2 The NJETS QCD Matrix Element Calculation

The NJETS Monte Carlo program [2] provides parton-level predictions based on the LO QCD $2 \rightarrow N$ matrix elements. The calculation requires the minimum separation between the final state partons in (η, ϕ)-space to exceed ΔR_{MIN}. We have set $\Delta R_{MIN} = 0.9$, and have used the KMRSD0 structure function parameterization [9] with the renormalization scale chosen to be the average p_T of the outgoing partons. NJETS does not use a parton fragmentation model. Jet definitions and selection cuts are therefore applied to the final state partons. To enable a direct comparison between NJETS predictions and observed distributions we have smeared the final state parton energies in our NJETS calculations with the Gaussian jet energy resolution function:

$$\sigma_E = 0.1\ E\ . \tag{1}$$

This provides a good approximation to the CDF jet resolution function.

3.3 Phase-Space Model

We have used the GENBOD phase-space generator [10] to generate samples of Monte Carlo events for which the multijet systems uniformly populate the N-body phase-space. These phase-space Monte Carlo events were generated with single-jet masses distributed according to the single-jet mass distribution predicted by the HERWIG Monte Carlo program. In addition, the multijet mass distributions were generated according to the corresponding distributions obtained from the HERWIG Monte Carlo calculation. Comparisons between the resulting phase-space model distributions and the corresponding HERWIG and NJETS Monte Carlo distributions help us to understand which multijet parameters are most sensitive to the behaviour of QCD multijet matrix elements.

4 Multijet Variables

To completely specify a system of N jets in the N-jet rest-frame we require (4N-3) independent parameters. However, the N-jet system can be rotated about the beam direction without losing any interesting information. Hence we need only specify (4N-4) parameters. We will use the N-jet mass and the (4N-5) dimensionless variables introduced and discussed in Ref. [4]. In the following the variables are briefly reviewed.

4.1 Three-Jet Variables

In previous three-jet analyses [11, 6, 12] it has become traditional to label the incoming interacting partons 1 and 2, and the outgoing jets 3, 4, and 5, with the jets ordered such that $E_3 > E_4 > E_5$, where E_j is the energy of jet j in the three-body rest-frame. At fixed three-jet mass m_{3J} a system of three massless jets can be specified in the three-jet rest-frame using four dimensionless variables, $X_3, X_4, \cos\theta_3$, and ψ_3, which are defined:

(i) The Dalitz variables X_3 and X_4:

$$X_j \equiv \frac{2\,E_j}{m_{3J}} \, . \tag{2}$$

(ii) The cosine of the leading jet scattering angle:

$$\cos\theta_3 \equiv \frac{\overrightarrow{P}_{AV} \cdot \overrightarrow{P}_3}{|\overrightarrow{P}_{AV}||\overrightarrow{P}_3|} \, , \tag{3}$$

where the average beam direction:

$$\overrightarrow{P}_{AV} \quad = \quad \overrightarrow{P}_1 - \overrightarrow{P}_2 \; , \tag{4}$$

and particle 1 is the incoming interacting parton with the highest energy in the laboratory frame.

(iii) ψ_3, defined in the three-jet rest-frame as the angle between the three-jet plane and the plane containing the leading-jet and the average beam direction:

$$\cos\psi_3 \quad \equiv \quad \frac{(\overrightarrow{P}_3 \times \overrightarrow{P}_{AV}) \cdot (\overrightarrow{P}_4 \times \overrightarrow{P}_5)}{|\overrightarrow{P}_3 \times \overrightarrow{P}_{AV}||\overrightarrow{P}_4 \times \overrightarrow{P}_5|} \; . \tag{5}$$

To specify a system of three massive jets we must supplement the traditional three-jet variables with three additional parameters that describe the single-jet masses. These parameters are taken to be the single-jet mass fractions f_3, f_4, and f_5, where:

$$f_j \quad \equiv \quad \frac{m_j}{m_{3J}} \; . \tag{6}$$

Thus we have eight three-jet variables which consist of m_{3J}, four parameters that specify the three-jet configuration ($X_3, X_4, \cos\theta_3$, and ψ_3), and three variables that specify the single-jet masses (f_3, f_4, and f_5).

4.2 Four-Jet and Five-Jet Variables

A multijet system with more than three-jets can be partially specified using the three-jet variables described above. This is accomplished by first reducing the multijet system to a three-body system. A four-jet system is reduced to a three-body system by combining the two-jets with the lowest two-jet mass. The resulting three-body system can then be described using the variables m_{4J}, $X_{3'}, X_{4'}, \cos\theta_{3'}$, $\psi_{3'}$, $f_{3'}, f_{4'}$, and $f_{5'}$, where the primes remind us that two jets have been combined. A five-jet system is reduced to a three-body system by first combining the two-jets with the lowest two-jet mass to obtain a four-body system, and then combining the two bodies with the lowest two-body mass to obtain a three-body system. The resulting three-body system can then be described using the variables m_{5J}, $X_{3''}, X_{4''}, \cos\theta_{3''}$, $\psi_{3''}$, $f_{3''}, f_{4''}$, and $f_{5''}$.

To complete the description of four-jet (five-jet) events we must now specify a further four (eight) variables that describe how the multijet system has been reduced to a three-body system. Consider first the step in which a four-body system is reduced to a three-body system. We label the two objects being combined A and B with $E_A > E_B$, where E_A and E_B are energies in the four-body rest-frame. To describe the (AB)-system we use the following four variables:

(a) The normalized masses f_A and f_B:

$$f_A \equiv \frac{m_A}{m_{NJ}} \quad \text{and} \quad f_B \equiv \frac{m_B}{m_{NJ}} \,, \tag{7}$$

where m_{NJ} is the mass of the multijet system.

(b) The two-body energy sharing variable X_A, defined in the multijet rest-frame as the fraction of the energy of the (AB)-system taken by A:

$$X_A \equiv \frac{E_A}{E_A + E_B} . \tag{8}$$

(c) The two-body angular variable ψ'_{AB}, defined in the multijet rest-frame as the angle between (i) the plane containing the (AB)-system and the average beam direction, and (ii) the plane containing A and B. The prime reminds us that in order to define ψ'_{AB} we have combined two bodies to obtain the (AB)-system. Note that:

$$\cos\psi'_{AB} \equiv \frac{(\overrightarrow{P}_A \times \overrightarrow{P}_B)\cdot(\overrightarrow{P}_{AB} \times \overrightarrow{P}_{AV})}{|\overrightarrow{P}_A \times \overrightarrow{P}_B||\overrightarrow{P}_{AB} \times \overrightarrow{P}_{AV}|} . \tag{9}$$

For five-jet events we must also specify the step in which the five-jet system is reduced to a four-body system. We label the two jets that are combined C and D with $E_C > E_D$, and use the four variables f_C, f_D, X_C, and ψ''_{CD}.

In summary, a four-jet system is described using 12 variables: m_{4J}, $X_{3'}$, $X_{4'}$, $\cos\theta_{3'}$, $\psi_{3'}$, $f_{3'}$, $f_{4'}$, $f_{5'}$, f_A, f_B, X_A, and ψ'_{AB}. A five-jet system is described using 16 variables: m_{5J}, $X_{3''}$, $X_{4''}$, $\cos\theta_{3''}$, $\psi_{3''}$, $f_{3''}$, $f_{4''}$, $f_{5''}$, $f_{A'}$, $f_{B'}$, $X_{A'}$, $\psi''_{A'B'}$, f_C, f_D, X_C, and ψ''_{CD}. Note that following the convention of Ref. [4] the primes indicate which parameters are defined after one or two steps in which two objects have been combined.

5 Results

The (4N-4) multijet variables described in the previous sections provide a set of independent parameters that span the multijet parameter space in the multijet rest frame. In the following the (4N-4) multijet distributions are compared with QCD and phase-space model predictions. All distributions are inclusive. If there are more than N jets in an event, the N highest E_T jets are used to define the multijet system. It should be noted that at fixed multijet mass the $\sum E_T > 420$ GeV, $\Delta R \geq 0.9$, and $E_T > 20$ GeV requirements place restrictions on the available multijet parameter space. Consequently, some regions of parameter space are depopulated due to a low experimental acceptance. These inefficient regions can be largely avoided in the three-jet analysis by placing suitable requirements on the multijet mass, leading-jet angle, and leading-jet Dalitz variable. In the following we have required that $m_{3J} > 600$ GeV/c^2, $|\cos\theta_3| < 0.6$, and $X_3 < 0.9$. These requirements select 1021 events with three-or-more jets, of which 320 events have more than three jets. Events entering the inclusive four-jet distributions are required to have $m_{4J} > 650$ GeV/c^2, $|\cos\theta_{3'}| < 0.8$, and $X_{3'} < 0.9$. These requirements select 1273 events with four-or-more jets, of which 245 events have more than four jets. Only 226 events enter into both the inclusive three-jet and inclusive four-jet distributions.. Note that the four-jet requirements reduce, but do not completely eliminate, the regions of low experimental acceptance. A more restrictive $X_{3'}$ requirement could be used to remove events populating the remaining region of low acceptance, but would cost a large reduction in statistics. Given the limited statistics of the present data sample, we have chosen to tolerate some regions of low experimental acceptance and use the phase-space model predictions to understand which regions of parameter space are affected. Finally, the inclusive five-jet data sample has very limited statistics, and we have therefore chosen to apply only the requirement $m_{5J} > 750$ GeV/c^2 to events entering the five-jet distributions. This requirement selects 817 events with five-or-more jets, of which 146 events have more than five jets. Only 148 events enter into both the five-jet and four-jet distributions, and only 42 events enter into both the five-jet and three-jet distributions.

5.1 Multijet Mass Distributions

In Ref. [1] HERWIG and NJETS QCD calculations were shown to give a good description of the shapes of the observed multijet mass distributions for exclusive samples of high-mass multijet events. In Figs. 1a, 1b, and 1c both the HERWIG and NJETS predictions are shown to give good descriptions of the shapes of the inclusive m_{3J}, m_{4J}, and m_{5J} distributions for the high-mass multijet samples described in this paper. Note that over the limited mass range of the present data sample, to a good approximation the m_{NJ} distributions are falling exponentially with increasing mass.

5.2 Three-Body Dalitz Distributions

We begin by considering the inclusive three-jet Dalitz distributions. Event populations in the (X_3, X_4)-plane are shown in Fig. 2 for (a) data, (b) NJETS, (c) HERWIG, and (d) phase-space model predictions. The phase-space population is uniform over the kinematically allowed region. Neither the data nor the QCD predictions exhibit large density variations in the (X_3, X_4)-plane in the region of interest ($X_3 < 0.9$), although with the relatively high statistical precision of the NJETS predictions the tendency for the predicted event density to increase as X_4 becomes large is visible (note that as $X_4 \rightarrow 1$ the third-to-leading jet Dalitz variable $X_5 \rightarrow 0$). The observed X_3 distribution is compared with phase-space model and QCD predictions in Fig. 3a. The corresponding comparisons for the X_4 distribution are shown in Fig. 3b. The HERWIG and NJETS predictions give reasonable descriptions of the observed distributions. Note that the observed distributions are not very different from the phase-space model predictions.

We next consider the inclusive four-jet distributions. Event populations in the ($X_{3'}$, $X_{4'}$)-plane are shown in Fig. 4 for (a) data, (b) NJETS, (c) HERWIG, and (d) phase-space model predictions. The phase-space population is not uniform over the kinematically allowed region. Care must therefore be taken in interpreting the distributions. The data and the QCD predictions exhibit a more uniform event density over the ($X_{3'}$, $X_{4'}$)-plane. The observed $X_{3'}$ distribution is compared with phase-space model and QCD predictions in Fig. 5a. The corresponding comparisons for the $X_{4'}$ distribution are shown in Fig. 5b. The HERWIG and NJETS predictions give reasonable descriptions of the observed distributions. Note that compared to the phase-space model predictions, the data and QCD predictions prefer topologies with large $X_{3'}$ and large $X_{4'}$ (note that as $X_{3'} \rightarrow 1$ the three-body topology approaches a two-body configuration, and as $X_{4'} \rightarrow 1$ we have $X_{5'} \rightarrow 0$).

Finally, consider the inclusive five-jet distributions. Event populations in the ($X_{3''}$, $X_{4''}$)-plane are shown in Fig. 6 for (a) data, (b) NJETS, (c) HERWIG, and (d) phase-space model predictions. Again, the phase-space population is not uniform over the kinematically allowed region, and care must be taken in interpreting the distributions. The observed event population and the QCD predictions are more uniformly distributed over the ($X_{3''}$, $X_{4''}$)-plane. However, all distributions are depleted as $X_{3''} \rightarrow 1$ and $X_{4''} \rightarrow 1$. The observed $X_{3''}$ distribution is compared with phase-space model and QCD predictions in Fig. 7a. The corresponding comparisons for the $X_{4''}$ distribution are shown in Fig. 7b. The HERWIG and NJETS predictions give reasonable descriptions of the observed distributions. Note that compared to the phase-space model predictions, the data and QCD predictions prefer topologies with $X_{3''} \rightarrow 1$ and $X_{4''} \rightarrow 1$.

5.3 Three-Body Angular Distributions

We begin by considering the inclusive three-jet angular distributions. Event populations in the ($\cos\theta_3$, ψ_3)-plane are shown in Fig. 8 for (a) data, (b) NJETS, (c) HERWIG, and (d) phase-space model predictions. The phase-space population is approximately uniform. In contrast both the observed distribution and the QCD predictions exhibit large density variations over the ($\cos\theta_3$, ψ_3)-plane, with the event density increasing as $|\cos\theta_3| \to 1$ and $\psi_3 \to 0$ or π. The increase in event rate as $|\cos\theta_3| \to 1$ is similar to the behaviour of the leading-jet angular distribution resulting from the $2 \to 2$ LO QCD matrix element. The increase in event rate as $\psi_3 \to 0$ or π reflects the preference of the three-jet matrix element for topologies which are planar. It is interesting to note that as $\cos\theta_3 \to 1$ the NJETS calculation shows a preference for configurations with $\psi_3 \to 0$ rather than π and as $\cos\theta_3 \to -1$ the NJETS calculation shows a preference for configurations with $\psi_3 \to \pi$ rather than 0. These preferred regions of the parameter space correspond to configurations in which jet 5 is closer to the beam direction, and therefore reflect the initial state radiation pole in the matrix element. The observed $\cos\theta_3$ distribution is compared with phase-space model and QCD predictions in Fig. 9a. The corresponding comparisons for the ψ_3 distribution are shown in Fig. 9b. Both HERWIG and NJETS predictions give reasonable descriptions of the observed distributions, which are very different from the phase-space model predictions. Note that the observed $\cos\theta_3$ distribution is also very similar to the LO prediction for $q\bar{q} \to q\bar{q}$ scattering [13].

Next, consider the inclusive four-jet angular distributions. Event populations in the ($\cos\theta_{3'}$, $\psi_{3'}$)-plane are shown in Fig. 10 for (a) data, (b) NJETS, (c) HERWIG, and (d) phase-space model predictions. The phase-space population is approximately uniform. In contrast both the observed distribution and the QCD predictions exhibit large density variations over the ($\cos\theta_{3'}$, $\psi_{3'}$)-plane, with the event density increasing as $|\cos\theta_{3'}| \rightarrow 1$ and $\psi_{3'} \rightarrow 0$ or π. This behaviour is similar to the behaviour of the corresponding three-jet distributions. The observed $\cos\theta_{3'}$ distribution is compared with phase-space model and QCD predictions in Fig. 11a. The corresponding comparisons for the $\psi_{3'}$ distribution are shown in Fig. 11b. Both HERWIG and NJETS predictions give reasonable descriptions of the observed distributions, which are very different from the phase-space model predictions. Note that the observed $\cos\theta_{3'}$ distribution is also very similar to the LO prediction for $q\overline{q} \rightarrow q\overline{q}$ scattering.

Finally, consider the inclusive five-jet angular distributions. Event populations in the ($\cos\theta_{3''}$, $\psi_{3''}$)-plane are shown in Fig. 12 for (a) data, (b) NJETS, (c) HERWIG, and (d) phase-space model predictions. The phase-space population is not uniform, and care must therefore be taken in interpreting the distributions. However, both the observed distribution and the QCD predictions exhibit much larger density variations over the ($\cos\theta_{3''}$, $\psi_{3''}$)-plane, with the event density increasing as $|\cos\theta_{3''}| \rightarrow 1$ and $\psi_{3''} \rightarrow 0$ or π. This behaviour is similar to the behaviour of the corresponding three-jet distributions. The observed $\cos\theta_{3''}$ distribution is compared with phase-space model and QCD predictions in Fig. 13a. The corresponding comparisons for the $\psi_{3''}$ distribution are shown in Fig. 13b. Both HERWIG and NJETS predictions give reasonable descriptions of the observed distributions, which are very different from the phase-space model predictions. Note that the observed $\cos\theta_{3''}$ distribution is also very similar to the LO prediction for $q\overline{q} \rightarrow q\overline{q}$ scattering even though there are now five jets in the final state.

5.4 Single-Body Mass Distributions for Three-Body Systems

The single-jet mass fraction distributions are shown in Fig. 14 for inclusive three-jet events. The f_j distributions are reasonably well described by the HERWIG Monte Carlo predictions, although there is a tendency for the HERWIG fragmentation model to slightly overestimate the fraction of low-mass jets. The observed distributions peak at $f_j \sim 0.05$ or less. Hence, for many purposes, jets at high energy can be considered to be massless. Note that since jets are massless in the matrix element calculations, there are no NJETS predictions for the f_j distributions.

The $f_{j'}$ and $f_{j''}$ distributions are shown for inclusive four-jet and inclusive five-jet events in Figs. 15 and 16 respectively. These distributions exhibit a single-jet peak at low mass-fractions (less than 0.05), and have a long tail associated with two-jet j' systems, and two-jet or three-jet j'' systems. The HERWIG predictions give a good description of all the distributions except perhaps at very low mass fractions (less than 0.05) where there is tendency to overestimate the observed jet rate. Although the NJETS calculations do not provide predictions for the single-jet part of the $f_{j'}$ and $f_{j''}$ distributions, they are seen to correctly predict the tail associated with multijet j' and j'' systems.

5.5 Two-Body Energy Sharing Distributions

The observed X_A distribution is shown in Figs. 17a and 17b to be reasonably well described by the HERWIG and NJETS predictions. The data and the QCD predictions favor a more asymmetric sharing of energy between the two jets A and B than predicted by the phase-space model. This reflects the presence of the soft gluon radiation pole in the QCD matrix element. In Figs. 17c and 17d the $X_{A'}$ distributions are shown to be qualitatively similar to the corresponding X_A distributions, and also similar to the corresponding X_C distributions shown in Figs. 17e and 17f. In general the data are reasonably well described by the QCD predictions and are very different from the phase-space model predictions.

5.6 Two-Body Angular Distributions

The observed ψ'_{AB} distribution is shown in Figs. 18a and 18b to be well described by the HERWIG and NJETS predictions. The phase-space model prediction is also approximately uniform, but underestimates the fraction of events in which the plane of the two-body system is close to the plane containing the two-body system and the beam direction ($\psi'_{AB} \to 0$ or π). In Figs. 18c and 18d the $\psi''_{A'B'}$ distributions are shown to be qualitively similar to the corresponding ψ'_{AB} distributions. The ψ''_{CD} distributions shown in Figs. 18e and 18f are similar to the phase-space model predictions. In all cases the data are well described by the QCD predictions. None of the observed distributions are very different from the phase-space model predictions, although the phase-space model calculation does underestimate the event rate as $\psi'_{AB} \to 0$ or π, or as $\psi''_{A'B'} \to 0$ or π.

5.7 Single-Body Mass Distributions for Two-Body Systems

The observed f_A, f_B, $f_{A'}$, $f_{B'}$, f_C, and f_D distributions are shown in Figs. 19a, 19b, 19c, 19d, 19e and 19f respectively to be reasonably well described by the HERWIG predictions although there is a tendency for the HERWIG predictions to overestimate the jet rate at very small single-jet masses. In all cases the distributions exhibit a single-jet mass peak at small mass fractions ($\sim$ 0.02 or less). The $f_{A'}$ and $f_{B'}$ have a long high-mass tail which corresponds to two-jet A' and B' systems. This tail is well described by the NJETS predictions.

5.8 χ^2 Test

In general both NJETS and HERWIG predictions give a good first description of the observed multijet distributions, which correspond to (4N-4) variables that span the N-body parameter space. A more quantitative assessment can be made by examining the χ^2 per degree of freedom that characterizes the agreement between the observed distributions and the QCD predictions. The χ^2 are listed for each distribution in Table 1. The computed χ^2's take into account statistical uncertainties on both measured points and the QCD Monte Carlo predictions, but do not take into account systematic uncertainties. In Ref. [1] the systematic uncertainties were mapped out for a limited set of multijet distributions, and found to be small compared to statistical uncertainties. Unfortunately, for the more complicated multijet parameter space of the present analysis, limited computing resources do not allow us to fully map out the systematic uncertainties on the predictions. However, even in the absence of a full evaluation of the systematic uncertainties, an examination of Table 1 shows that NJETS provides a reasonable description of all of the observed multijet distributions except perhaps the X_A distribution. The combined χ^2 for the NJETS description of all of the three-jet distributions $\chi^2/\mathrm{NDF} = 1.03$ (45 degrees of freedom). The corresponding result for the four-jet distributions is $\chi^2/\mathrm{NDF} = 1.47$ (63 degrees of freedom) if the X_A distribution is included in the comparison, and $\chi^2/\mathrm{NDF} = 1.24$ (55 degrees of freedom) if the X_A distribution is not included. The result for the combined five-jet distributions is $\chi^2/\mathrm{NDF} = 1.21$ (63 degrees of freedom). The observed distributions are described less well by the HERWIG parton shower Monte Carlo predictions, for which the X_4, $\cos\theta_{3'}$, $\psi_{3'}$, and $\cos\theta_{3''}$ distributions have χ^2s significantly poorer than those for the corresponding NJETS predictions. Restricting the comparison to those distributions predicted by both the NJETS and HERWIG calculations (i.e. all distributions except the single-body mass fraction distributions) we find the overall χ^2 per degree of freedom for the HERWIG comparison of the combined three-jet distributions is $\chi^2/\mathrm{NDF} = 1.58$ (45 degrees of freedom), for the combined four-jet distributions $\chi^2/\mathrm{NDF} = 1.63$ (63 degrees of freedom), and for the combined five-jet distributions $\chi^2/\mathrm{NDF} = 1.52$ (63 degrees of freedom).

6 Conclusions

The properties of high-mass three-jet, four-jet, and five-jet events produced at the Fermilab Tevatron proton-antiproton collider have been compared with NJETS LO QCD matrix element predictions, HERWIG QCD parton shower Monte Carlo predictions, and predictions from a model in which events are distributed uniformly over the available multibody phase-space. The phase-space model is unable to describe the shapes of multijet distributions in regions of parameter space where the QCD calculations predict large contributions from initial- and final-state gluon radiation. In contrast, the QCD predictions give a good first description of the observed multijet distributions, which correspond to (4N-4) variables that span the N-body parameter space. A more quantitative assessment based on the χ^2 per degree of freedom that characterizes the agreement between the observed distributions and the QCD predictions shows that NJETS gives a good description of all the distributions except perhaps the X_A distribution for four-jet events. The NJETS predictions seem to give a better description of the observed distributions than the HERWIG predictions. This is particularly true of the X_4, $\cos\theta_{3'}$, $\psi_{3'}$, and $\cos\theta_{3''}$ distributions. Finally, we do not see clear evidence for any deviation from the predicted multijet distributions that might indicate new phenomena associated with the presence of many hard partons in the final state. The general agreement between data, NJETS, and HERWIG suggests that $2 \rightarrow 2$ scattering plus gluon radiation provides a good first approximation to the full LO QCD matrix element for events with three, four, or even five jets in the final state.

Acknowledgements

We thank the Fermilab Accelerator Division and the technical and support staff of our respective institutions. This work was supported by the U.S. Department of Energy, the U.S. National Science Foundation, the Istituto Nazionale di Fisica Nucleare of Italy, the Ministry of Science, Culture and Education of Japan, the Natural Sciences and Engineering Research Council of Canada, and the A.P. Sloan Foundation.

References

[1] F. Abe et al. (CDF Collaboration), *Phys. Rev. Lett.* **75**, 608 (1995).

[2] F.A. Berends, W. Giele, and H. Kuijf, *Nucl. Phys.* **B333**, 120 (1990);
F.A. Berends, W. Giele, and H. Kuijf, *Phys. Lett.* **232B**, 266 (1990);
F.A. Berends and H. Kuijf, *Nucl. Phys.* **B353**, 59 (1991).

[3] G. Marchesini and B. Webber, *Nucl. Phys.* **B310**, 461 (1988).

[4] S. Geer and T. Asakawa, *Phys. Rev.* **D53**, 4793 (1996).

[5] F. Abe et al. (CDF Collaboration), *Nucl. Instr. and Meth.* **A271**, 387 (1988).

[6] F. Abe et al. (CDF Collaboration), *Phys. Rev.* **D45**, 1448 (1992).

[7] F. Abe et al. (CDF Collaboration), *Phys. Rev.* **D45**, 2249 (1992).

[8] H.L. Lai et al; Preprint MSU-HEP-41024, CTEQ-404, (to be published).

[9] A.D. Martin, R.G. Roberts, W.J. Stirling; *Phys. Lett.* **306B**, 145 (1993).

[10] CERN Program Library Manual 1989.10.03, Routine W515, p. 6.503.

[11] G. Arnison et al. (UA1 Collaboration), *Phys. Lett.* **158B**, 494 (1985).

[12] S. Abachi et al. (D0 Collaboration), *FERMILAB PUB-95/296-E* (1995) (to be published in Phys. Rev. D).

[13] B.L. Combridge, J. Kripfganz, and J. Ranft, *Phys. Lett.* **70B**, 234 (1977).

Variable	NDF	NJETS − DATA	HERWIG − DATA	NJETS − HERWIG
m_{3J}	6	1.55	1.10	0.45
X_3	8	0.15	1.56	2.35
X_4	6	2.03	3.27	3.41
$\cos\theta_3$	11	1.13	0.74	1.29
ψ_3	14	0.79	1.71	2.62
f_3	9	–	2.92	–
f_4	9	–	8.21	–
f_5	6	–	0.30	–
m_{4J}	6	0.98	1.14	0.29
$X_{3'}$	7	1.37	1.00	1.61
$X_{4'}$	6	0.85	0.41	1.79
$\cos\theta_{3'}$	15	1.27	2.28	1.98
$\psi_{3'}$	14	1.35	2.19	1.96
X_A	8	3.08	1.03	2.09
ψ'_{AB}	7	1.35	1.87	1.54
$f_{3'}$	11	–	3.18	–
$f_{4'}$	8	–	3.74	–
$f_{5'}$	8	–	1.90	–
f_A	13	–	2.20	–
f_B	11	–	4.07	–
m_{5J}	8	0.86	1.24	1.79
$X_{3''}$	7	0.98	0.80	1.28
$X_{4''}$	6	1.02	1.72	0.74
$\cos\theta_{3''}$	7	0.61	3.19	6.20
$\psi_{3''}$	7	0.68	1.85	2.11
$X_{A'}$	7	2.80	2.02	1.38
$\psi''_{A'B'}$	7	1.16	1.11	0.29
X_C	7	1.64	0.58	1.42
ψ''_{CD}	7	1.09	1.27	0.17
$f_{3''}$	12	–	4.11	–
$f_{4''}$	8	–	5.66	–
$f_{5''}$	8	–	2.82	–
f_C	10	–	1.30	–
f_D	7	–	5.95	–
$f_{A'}$	12	–	3.74	–
$f_{B'}$	12	–	1.57	–

Table 1: Statistical comparison of agreement between oberserved and predicted distributions. The χ^2 per degree of freedom are listed for comparisons of the various observed and QCD predicted distributions shown in the figures.

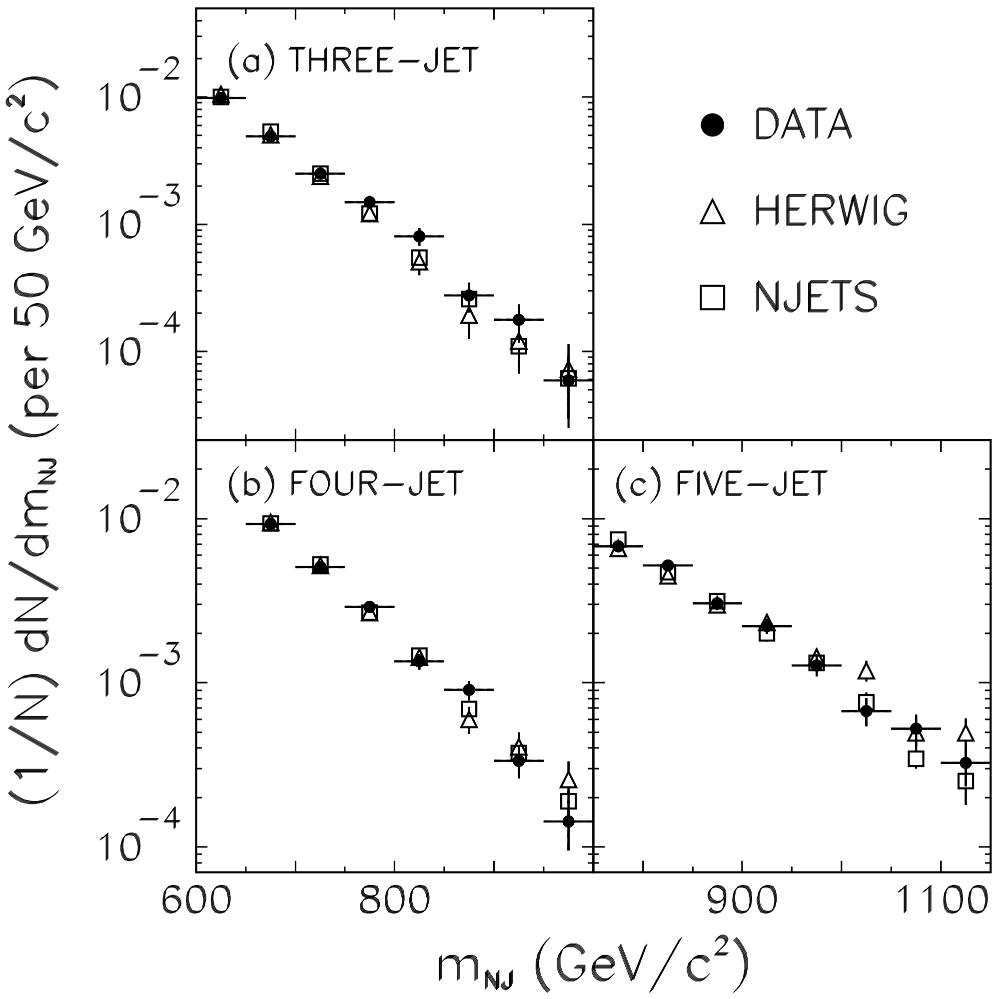

Figure 1: Inclusive multijet mass distributions for topologies with (a) three jets, (b) four jets, and (c) five jets. Observed distributions (points) are compared with HERWIG predictions (triangles) and NJETS predictions (squares).

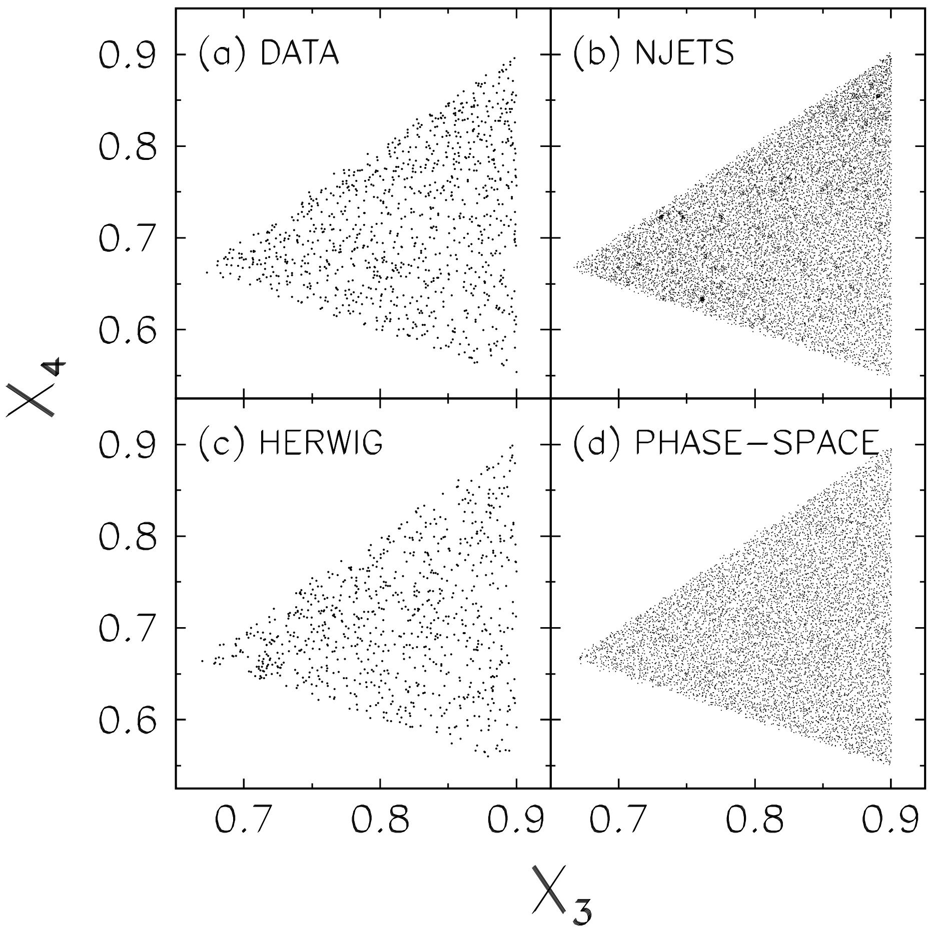

Figure 2: Three-jet Dalitz distributions after imposing the requirements $m_{3J} > 600$ GeV/c^2, $X_3 < 0.9$, and $|\cos\theta_3| < 0.6$, shown for (a) data, (b) NJETS, (c) HERWIG, and (d) the phase-space model.

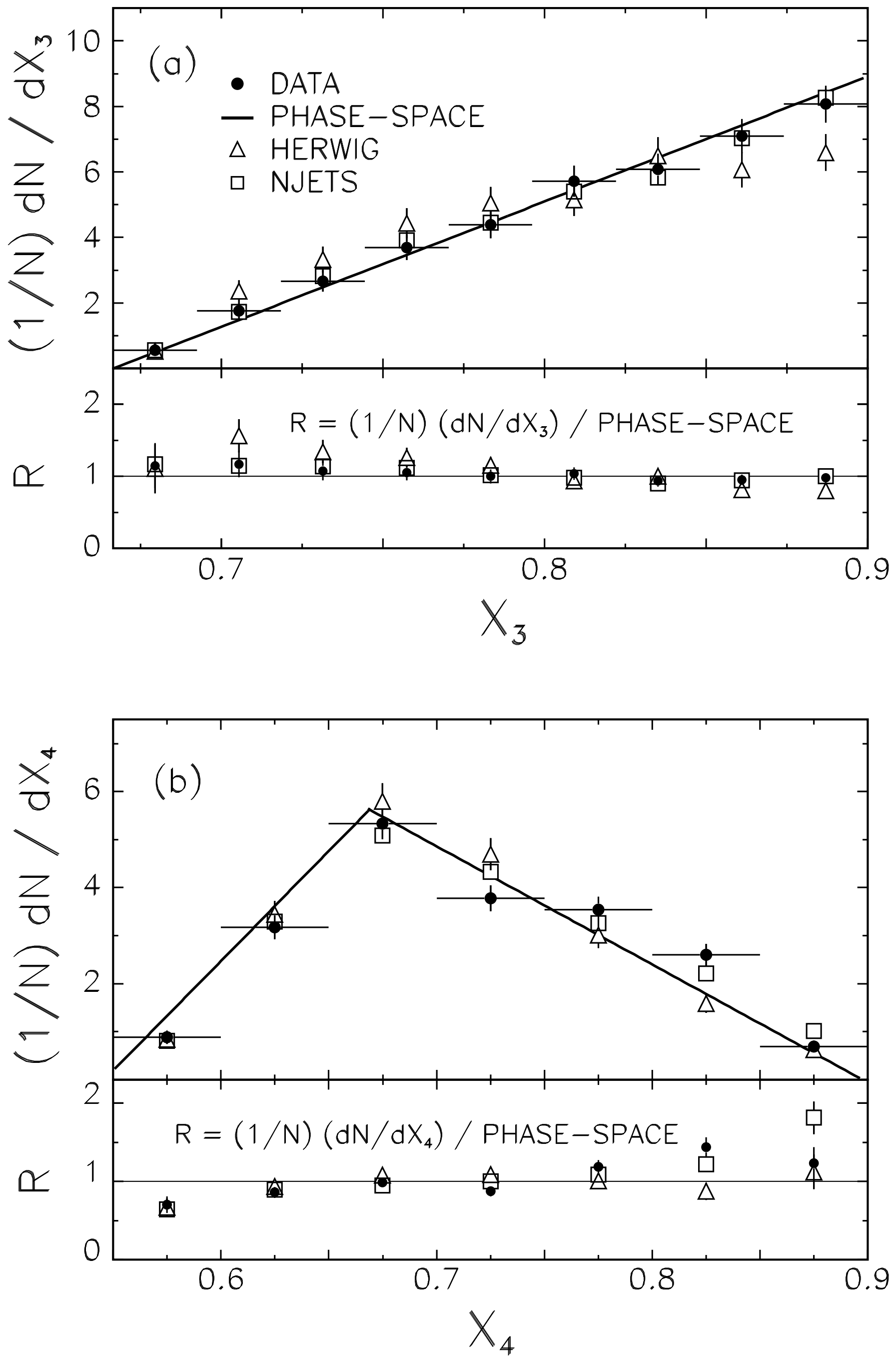

Figure 3: Inclusive three-jet Dalitz distributions for events that satisfy the requirements $m_{3J} > 600$ GeV$/c^2$, $X_3 < 0.9$, and $|\cos\theta_3| < 0.6$. Data (points) are compared with HERWIG predictions (triangles), NJETS predictions (squares), and phase-space model predictions (curves) for (a) X_3, and (b) X_4.

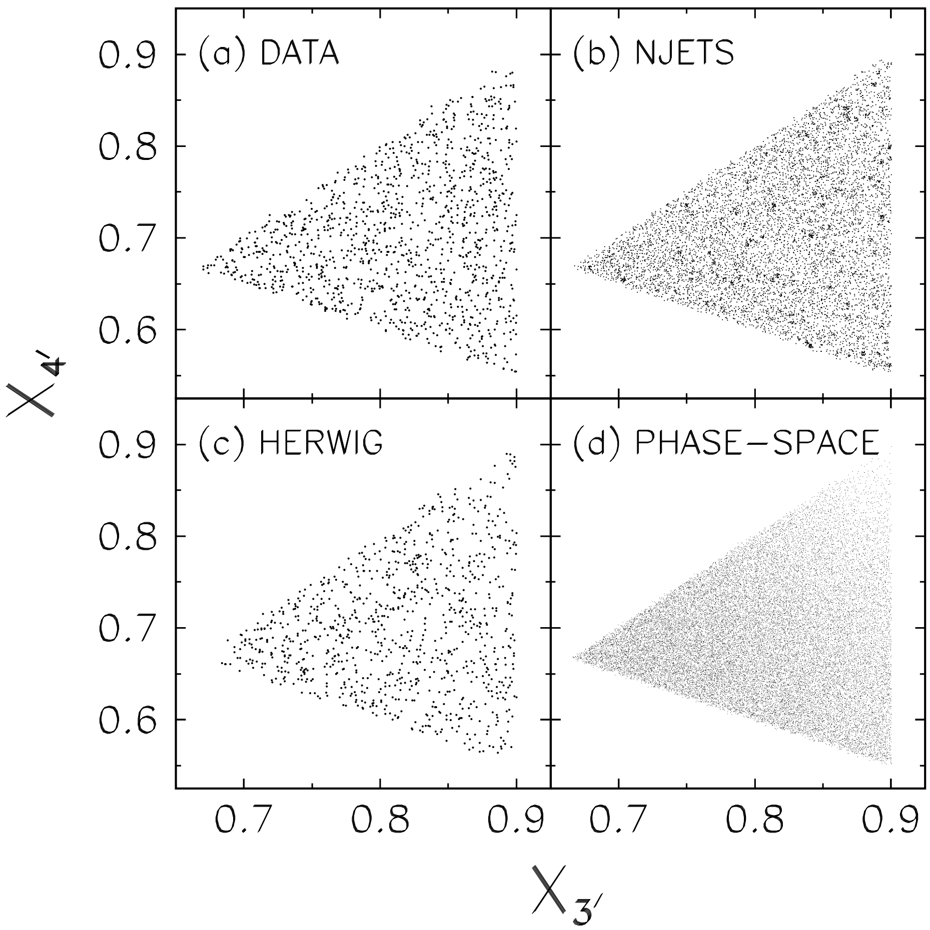

Figure 4: Inclusive four-jet Dalitz distributions for events that that satisfy the requirements $m_{4J} > 650$ GeV$/c^2$, $X_{3'} < 0.9$, and $|\cos\theta_{3'}| < 0.8$, shown for (a) data, (b) NJETS, (c) HERWIG, and (d) phase-space model predictions.

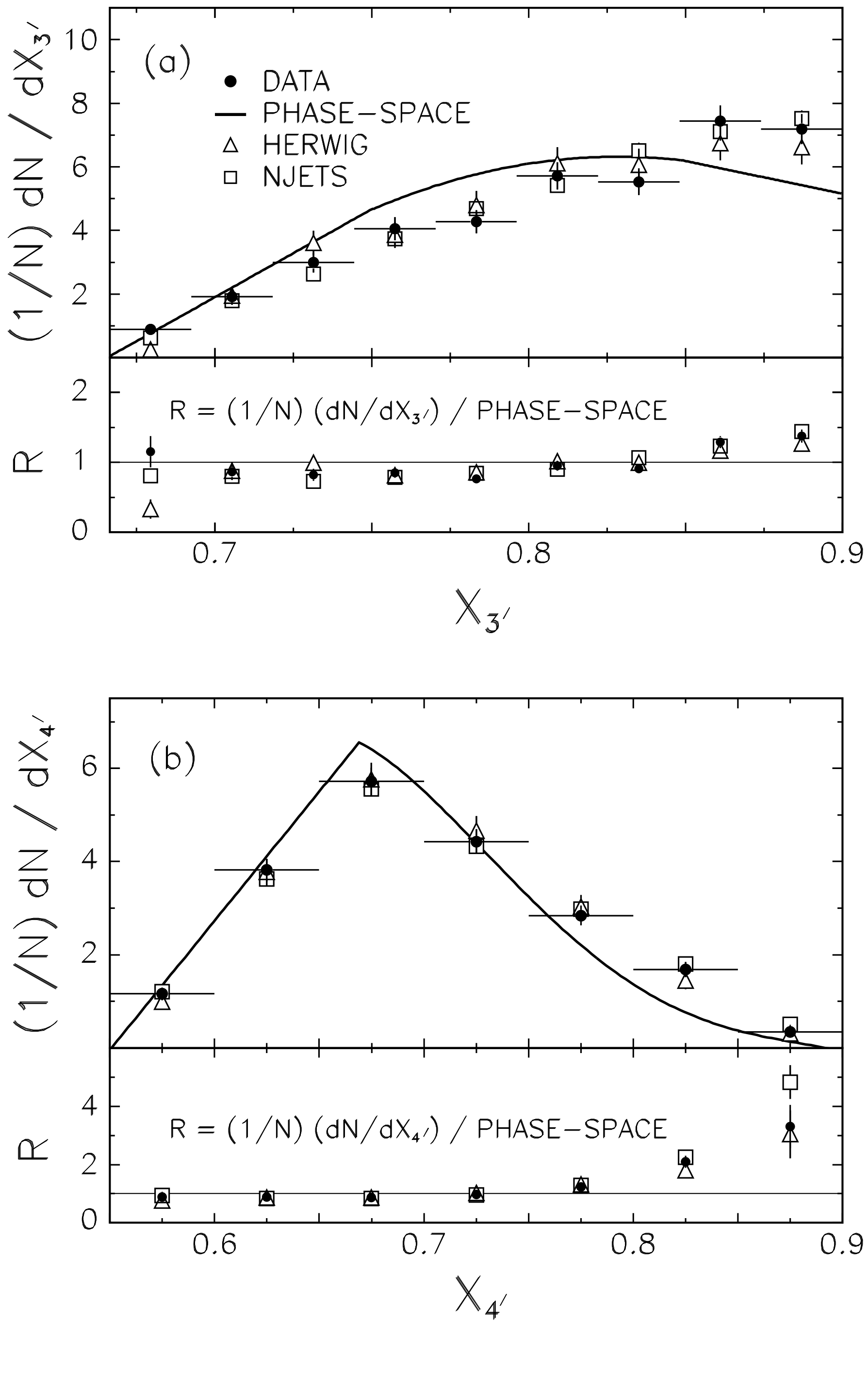

Figure 5: Dalitz distributions for inclusive four-jet topologies that satisfy the requirements $m_{4J} > 650$ GeV/c^2, $X_{3'} < 0.9$, and $|\cos\theta_{3'}| < 0.8$. Data (points) are compared with HERWIG predictions (triangles), NJETS predictions (squares), and phase-space model predictions (curves) for (a) $X_{3'}$, and (b) $X_{4'}$.

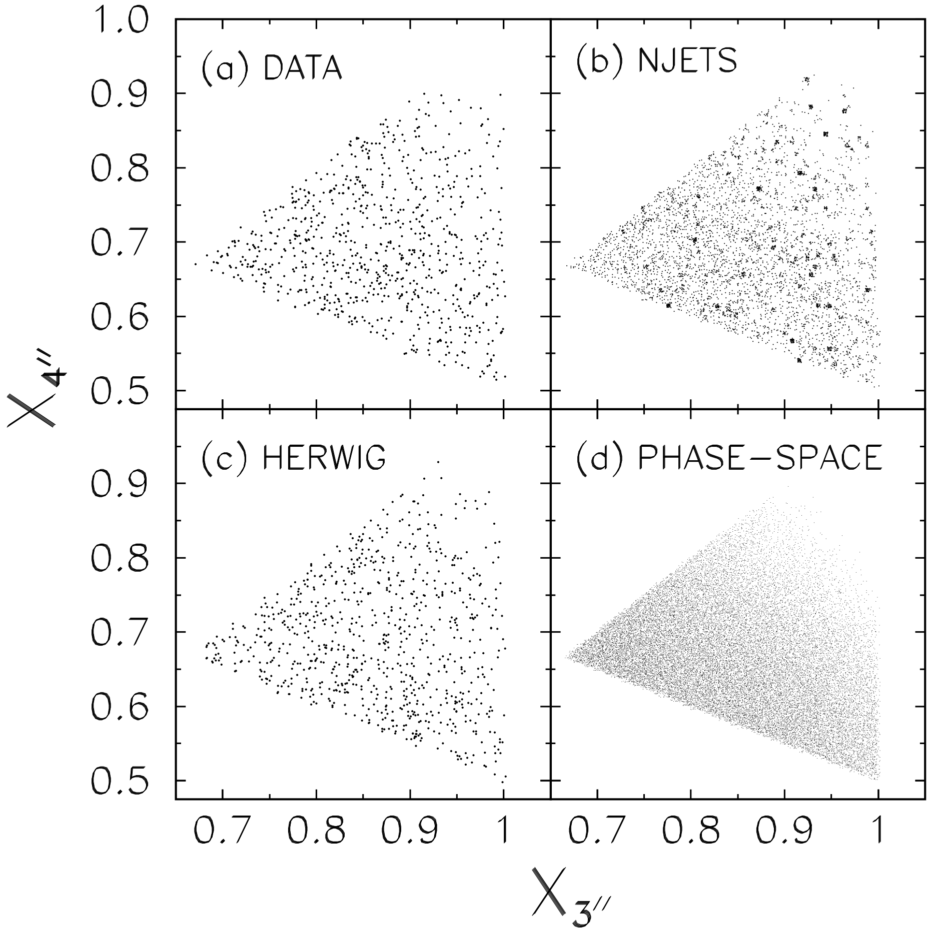

Figure 6: Inclusive five-jet Dalitz distributions for events that satisfy the requirement $m_{5J} > 750$ GeV$/c^2$, shown for (a) data, (b) NJETS, (c) HERWIG, and (d) phase-space model predictions.

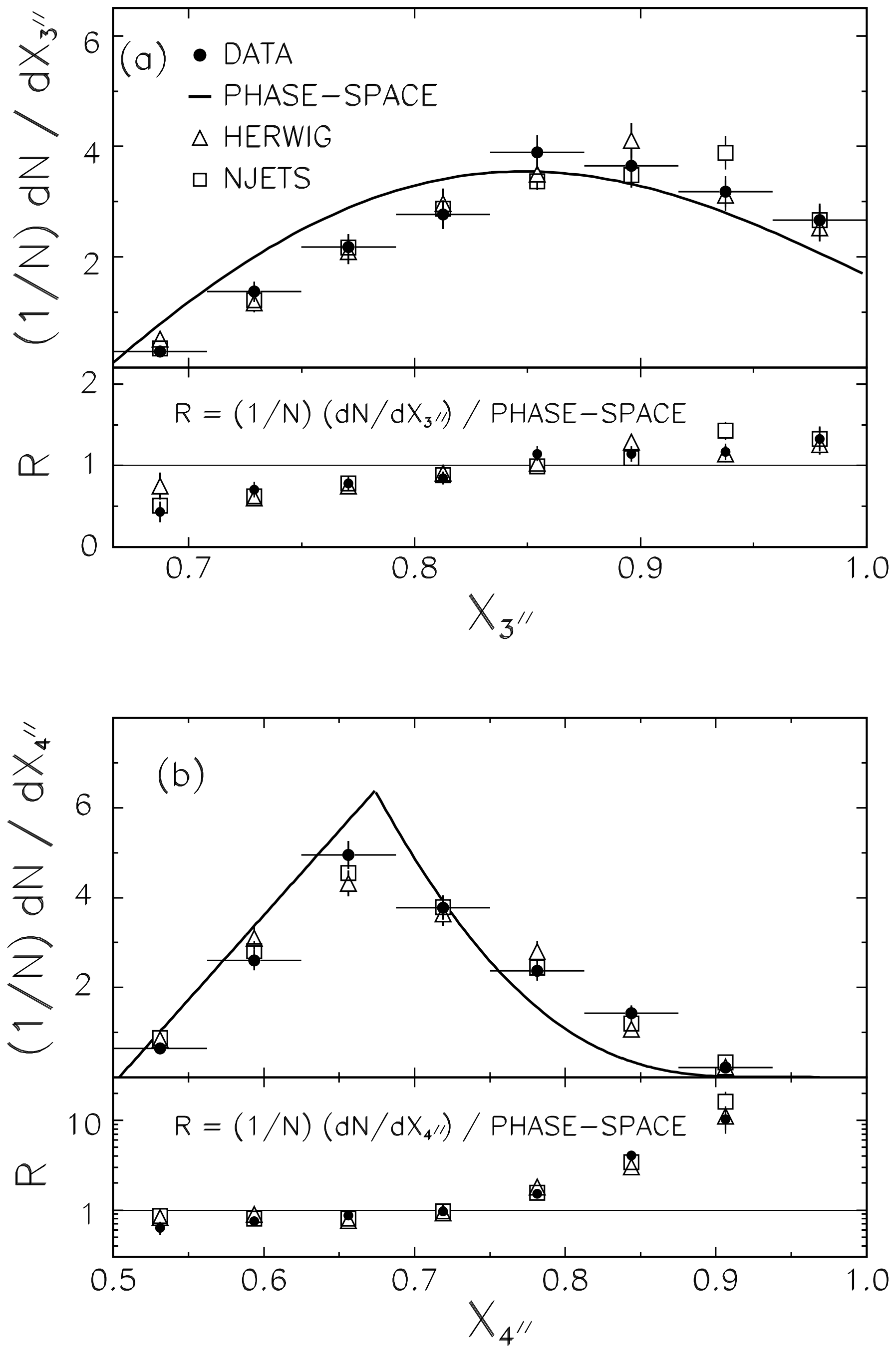

Figure 7: Dalitz distributions for inclusive five-jet topologies that satisfy the requirement $m_{5J} > 750$ GeV/c^2. Data (points) are compared with HERWIG predictions (triangles), NJETS predictions (squares), and phase-space model predictions (curves) for (a) $X_{3''}$, and (b) $X_{4''}$.

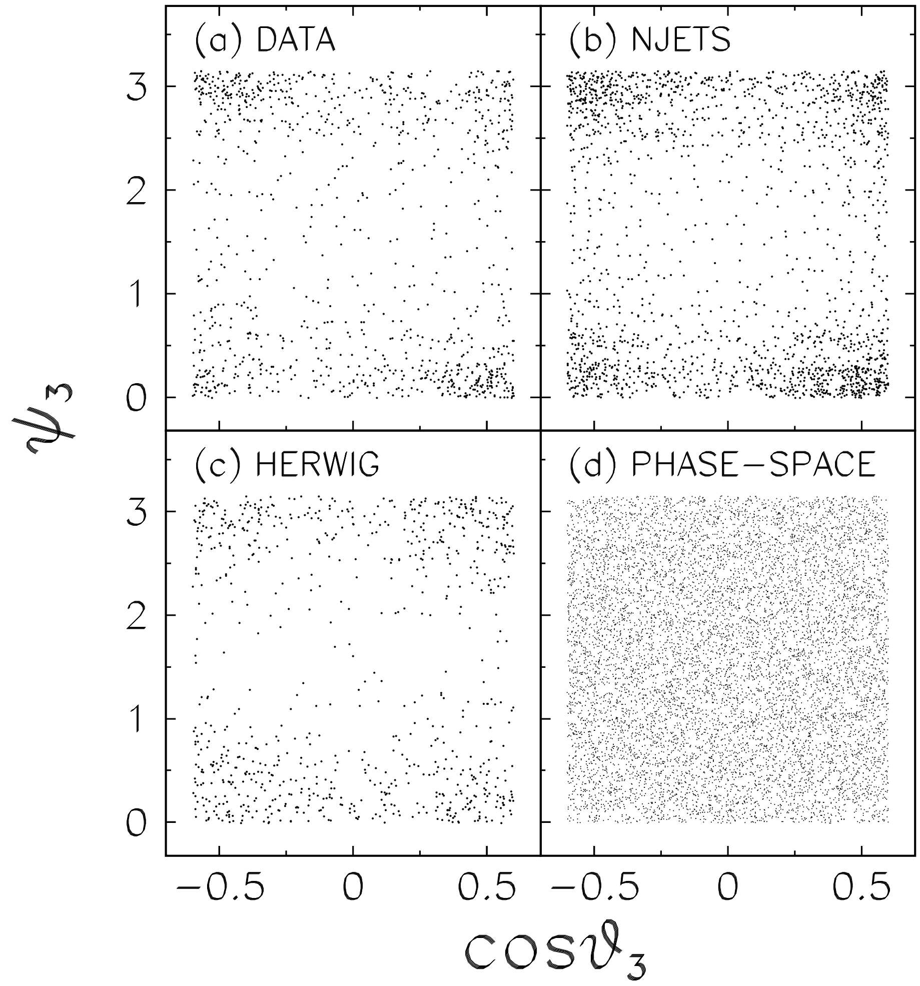

Figure 8: Inclusive three-jet angular distributions for events that satisfy the requirements $m_{3J} > 600$ GeV$/c^2$, $X_3 < 0.9$, and $|\cos\theta_3| < 0.6$. Event populations in the $(\cos\theta_3,\ \psi_3)$-plane are shown for (a) data, (b) NJETS, (c) HERWIG, and (d) phase-space model predictions.

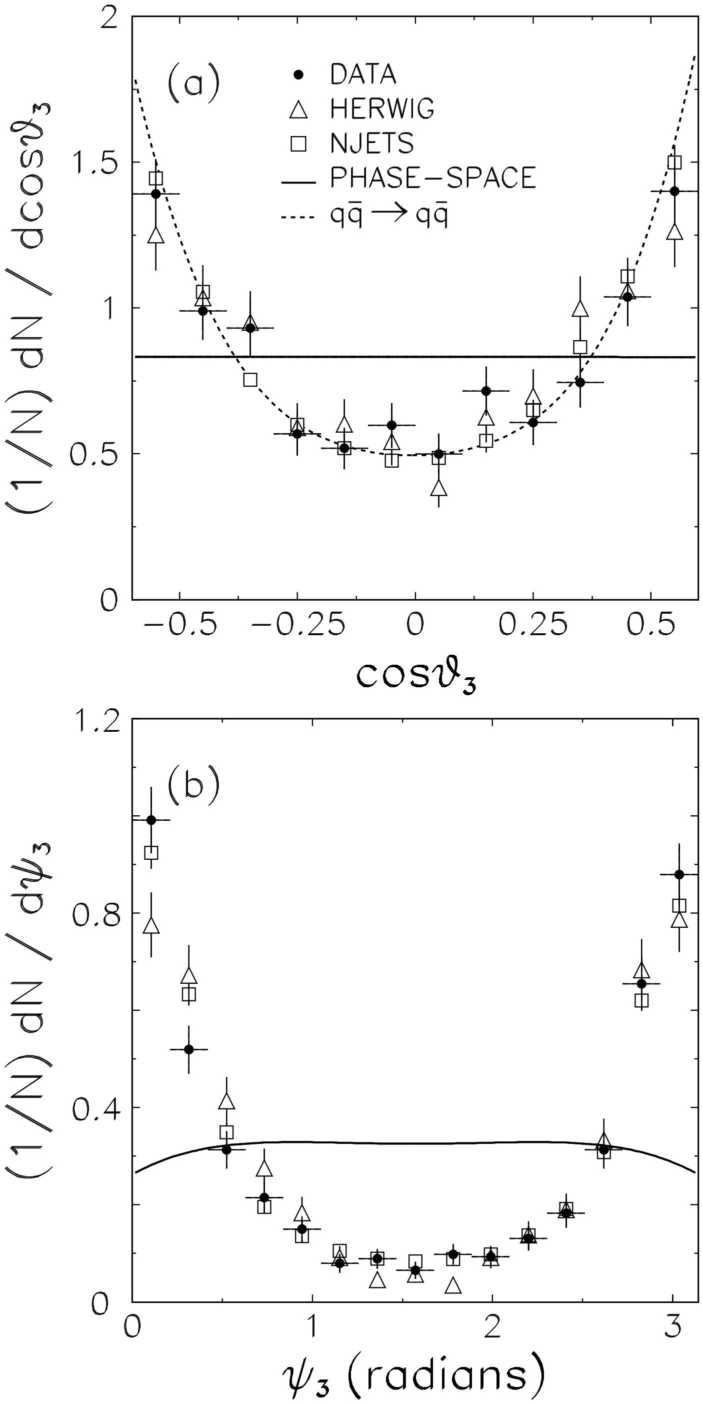

Figure 9: Inclusive three-jet angular distributions for events that satisfy the requirements $m_{3J} > 600$ GeV$/c^2$, $X_3 < 0.9$, and $|\cos\theta_3| < 0.6$. Data (points) are compared with HERWIG predictions (triangles), NJETS predictions (squares), and phase-space model predictions (curves) for (a) $\cos\theta_3$ and (b) ψ_3. The broken curve in the $\cos\theta_3$ figure is the LO QCD prediction for $q\overline{q} \to q\overline{q}$ scattering.

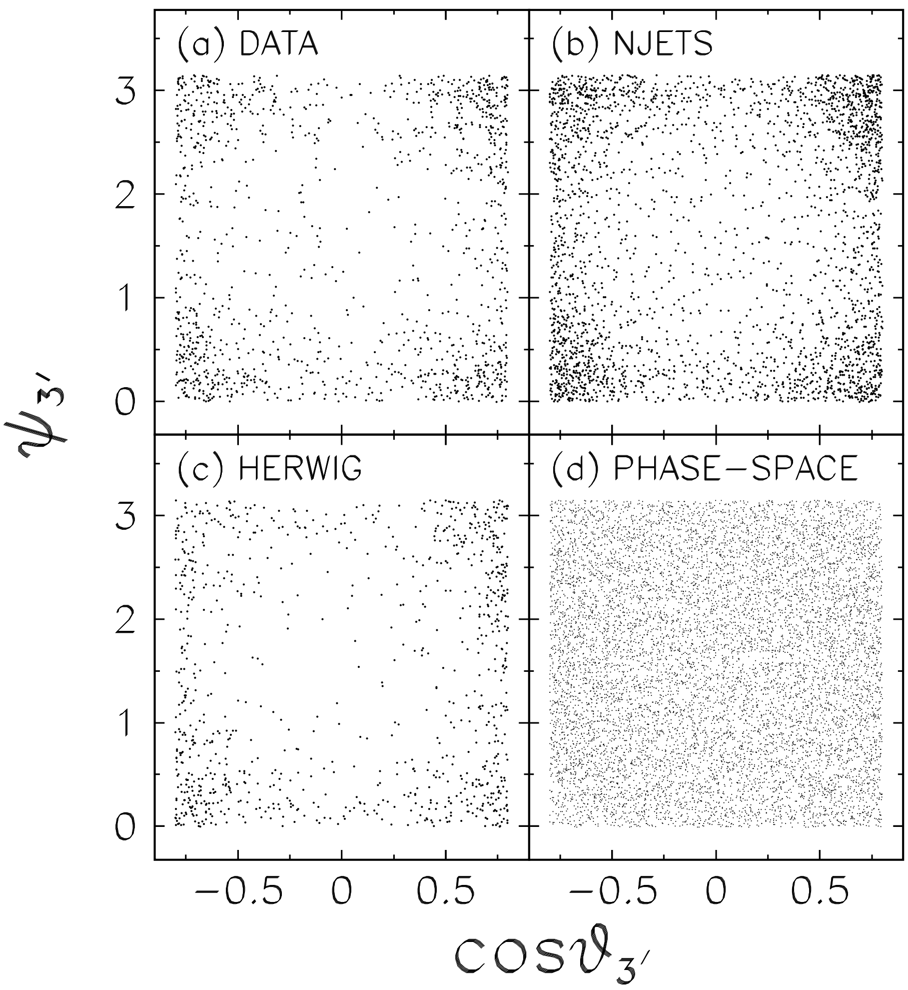

Figure 10: Inclusive four-jet angular distributions for events that satisfy the requirements $m_{4J} > 650$ GeV/c^2, $X_{3'} < 0.9$, and $|\cos\theta_{3'}| < 0.8$. Event populations in the ($\cos\theta_{3'}$, $\psi_{3'}$)-plane are shown for (a) data, (b) NJETS, (c) HERWIG, and (d) phase-space model predictions.

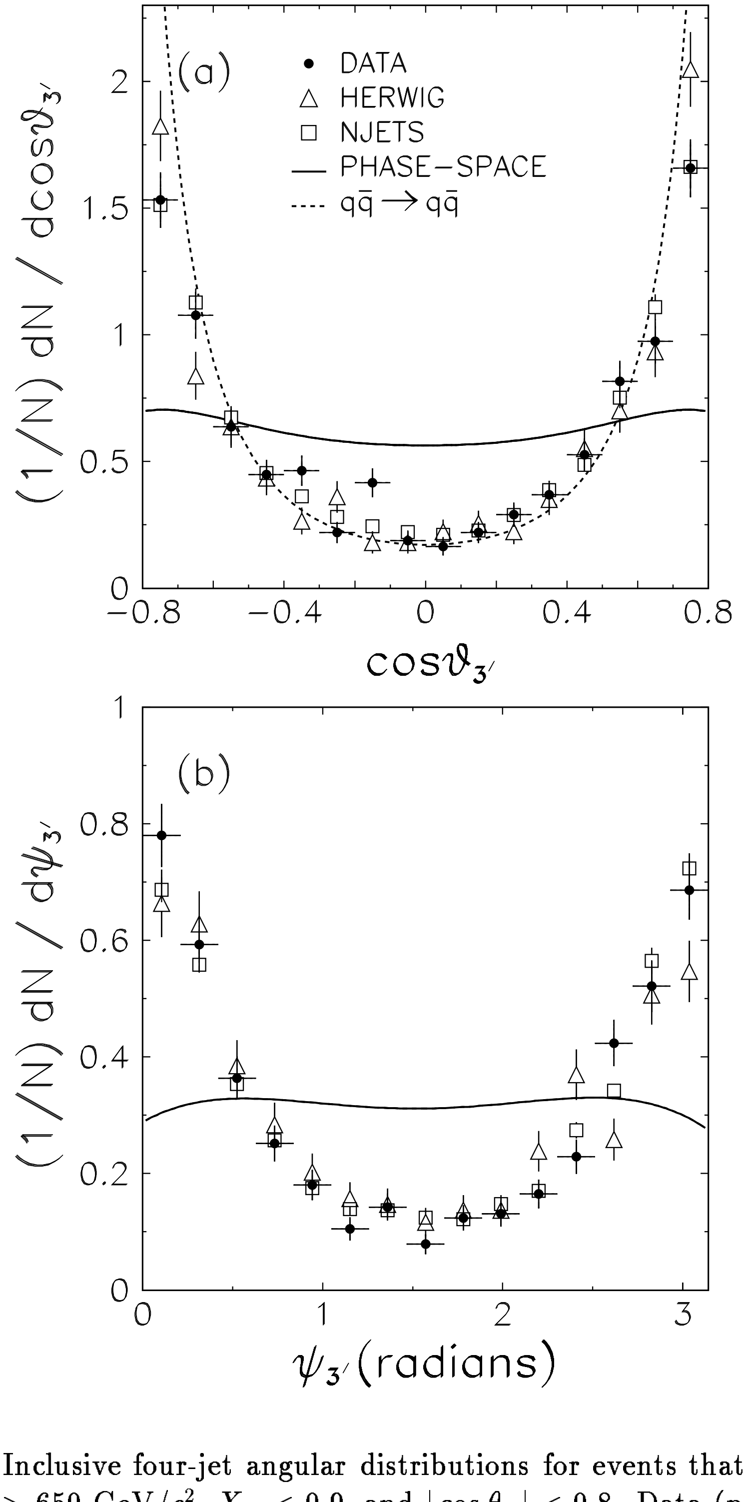

Figure 11: Inclusive four-jet angular distributions for events that satisfy the requirements $m_{4J} > 650$ GeV$/c^2$, $X_{3'} < 0.9$, and $|\cos\theta_{3'}| < 0.8$. Data (points) are compared with HERWIG predictions (triangles), NJETS predictions (squares), and phase-space model predictions (curves) for (a) $\cos\theta_{3'}$ and (b) $\psi_{3'}$. The broken curve in the $\cos\theta_{3'}$ figure is the LO QCD prediction for $q\overline{q} \to q\overline{q}$ scattering.

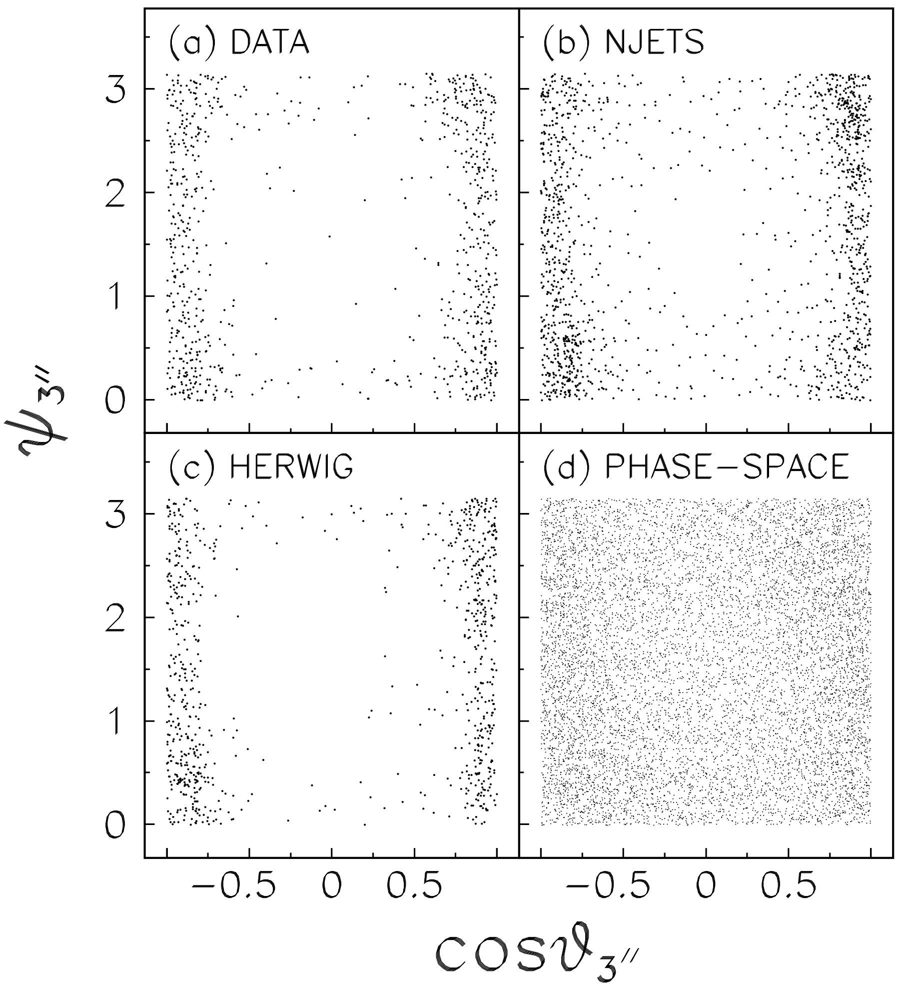

Figure 12: Inclusive five-jet angular distributions for events that satisfy the requirement $m_{5J} > 750$ GeV/c^2. Event populations in the ($\cos\theta_{3''}$, $\psi_{3''}$)-plane are shown for (a) data, (b) NJETS, (c) HERWIG, and (d) phase-space model predictions.

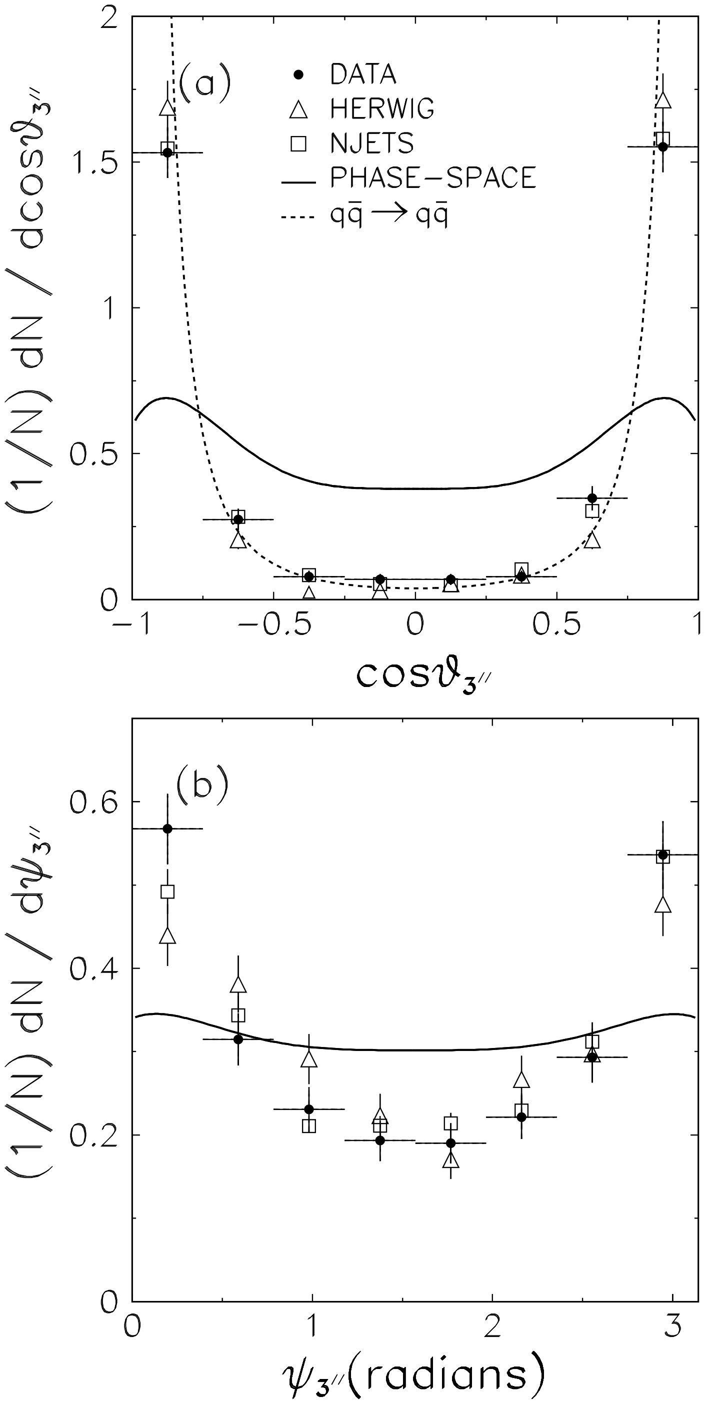

Figure 13: Inclusive five-jet angular distributions for events that satisfy the requirement $m_{5J} > 750$ GeV$/c^2$. Data (points) are compared with HERWIG predictions (triangles), NJETS predictions (squares), and phase-space model predictions (curves) for (a) $\cos\theta_{3''}$ and (b) $\psi_{3''}$. The broken curve in the $\cos\theta_{3''}$ figure is the LO QCD prediction for $q\bar{q} \rightarrow q\bar{q}$ scattering.

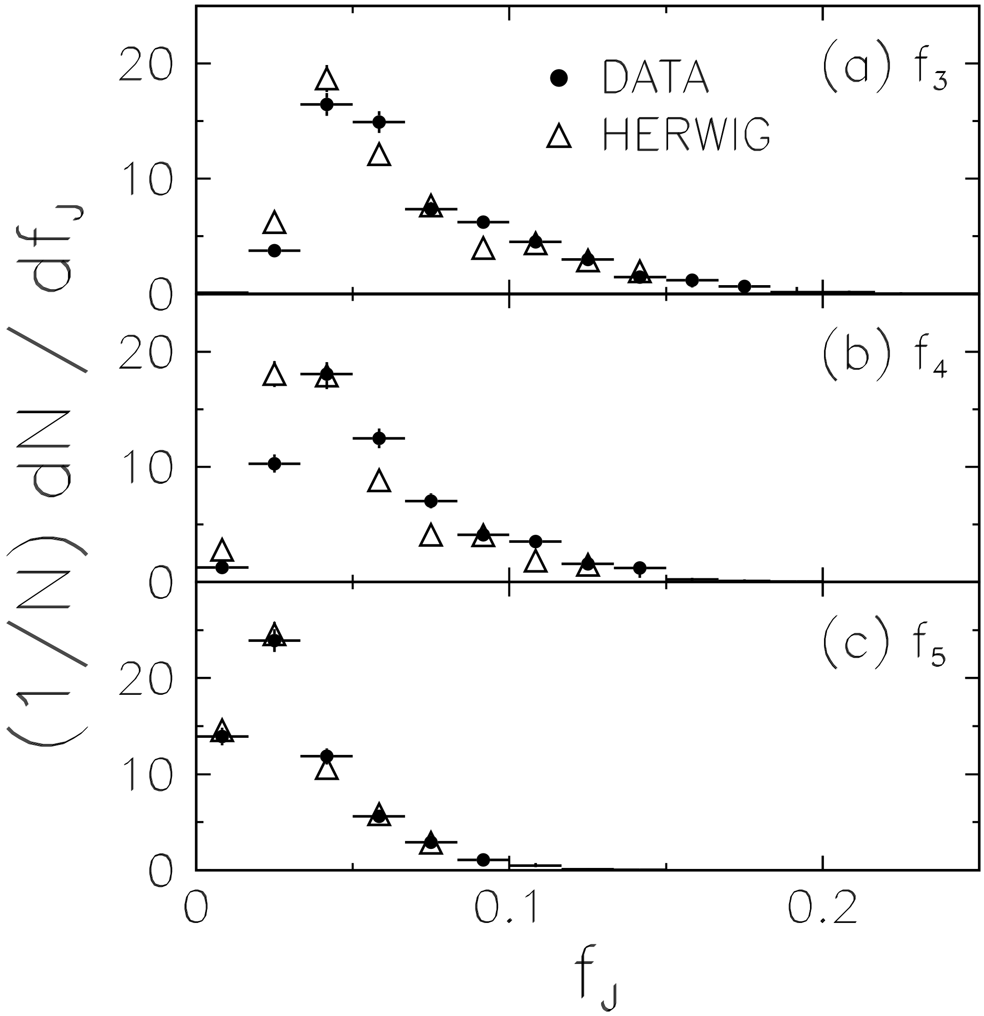

Figure 14: Single-jet mass fraction distributions for inclusive three-jet events. Data (points) compared with HERWIG predictions (triangles), shown for (a) the highest energy jet in the three-jet rest-frame, (b) the second-to-highest energy jet, and (c) the third-to-highest energy jet.

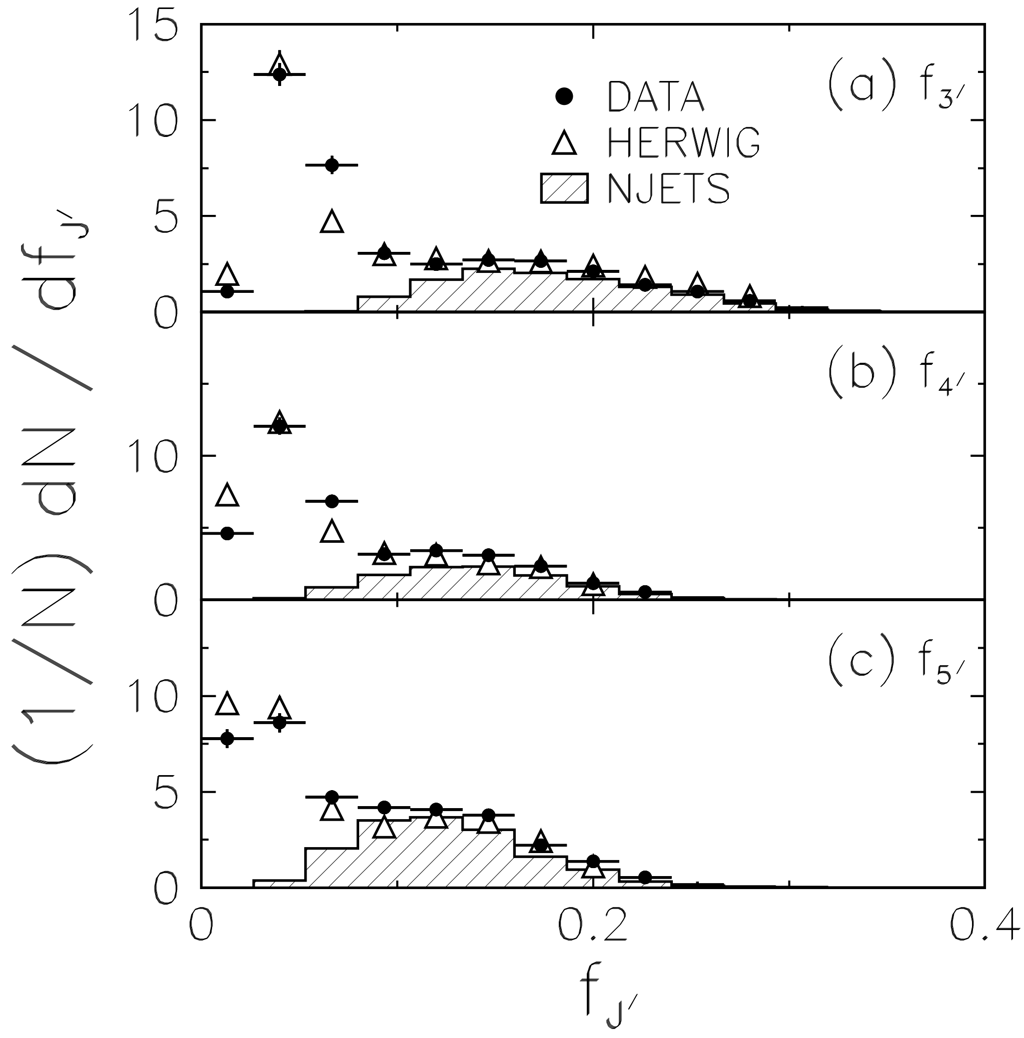

Figure 15: Single-body mass fraction distributions for inclusive four-jet events. Data (points) compared with HERWIG predictions (triangles), and NJETS predictions (histograms), shown for (a) the highest energy body in the three-body rest-frame, (b) the second-to-highest energy body, and (c) the third-to-highest energy body.

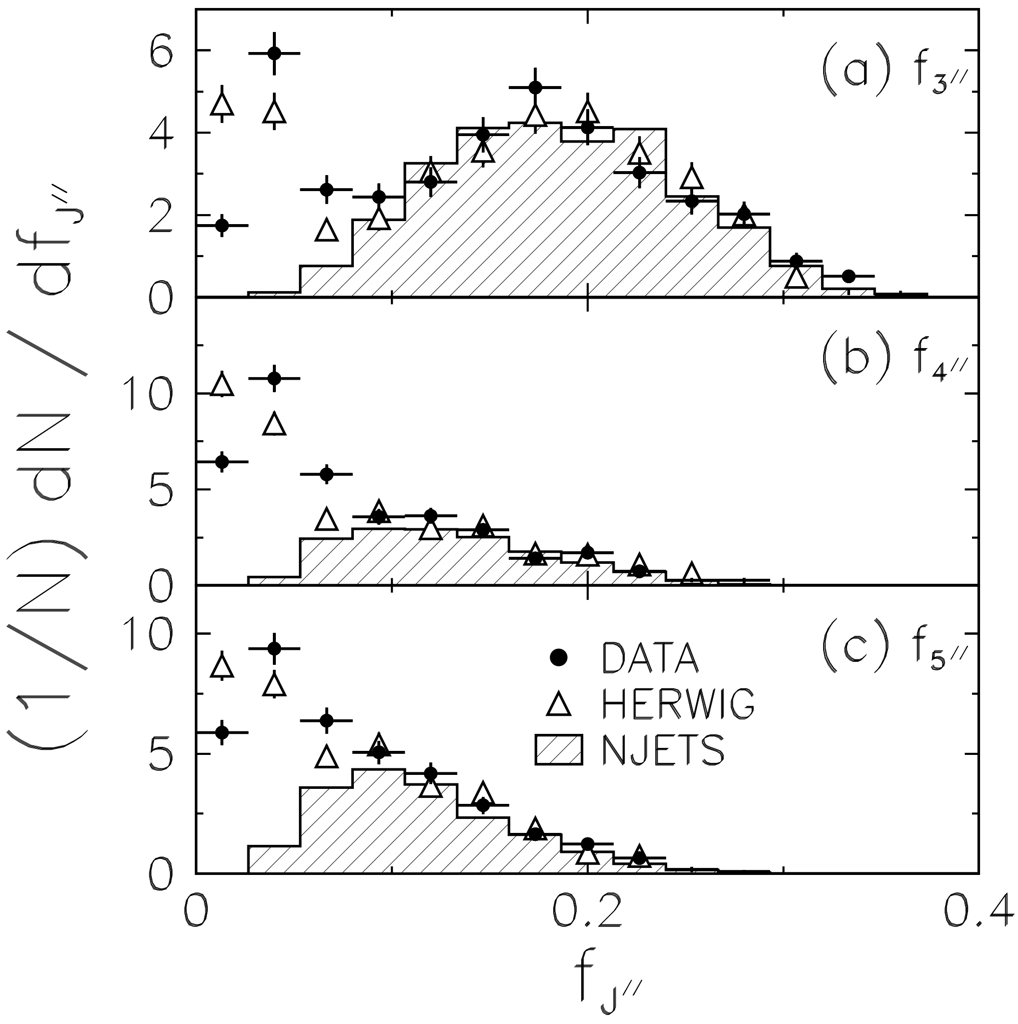

Figure 16: Single-body mass fraction distributions for inclusive five-jet events. Data (points) compared with HERWIG predictions (triangles), and NJETS predictions (histograms), shown for (a) the highest energy body in the three-body rest-frame, (b) the second-to-highest energy body, and (c) the third-to-highest energy body.

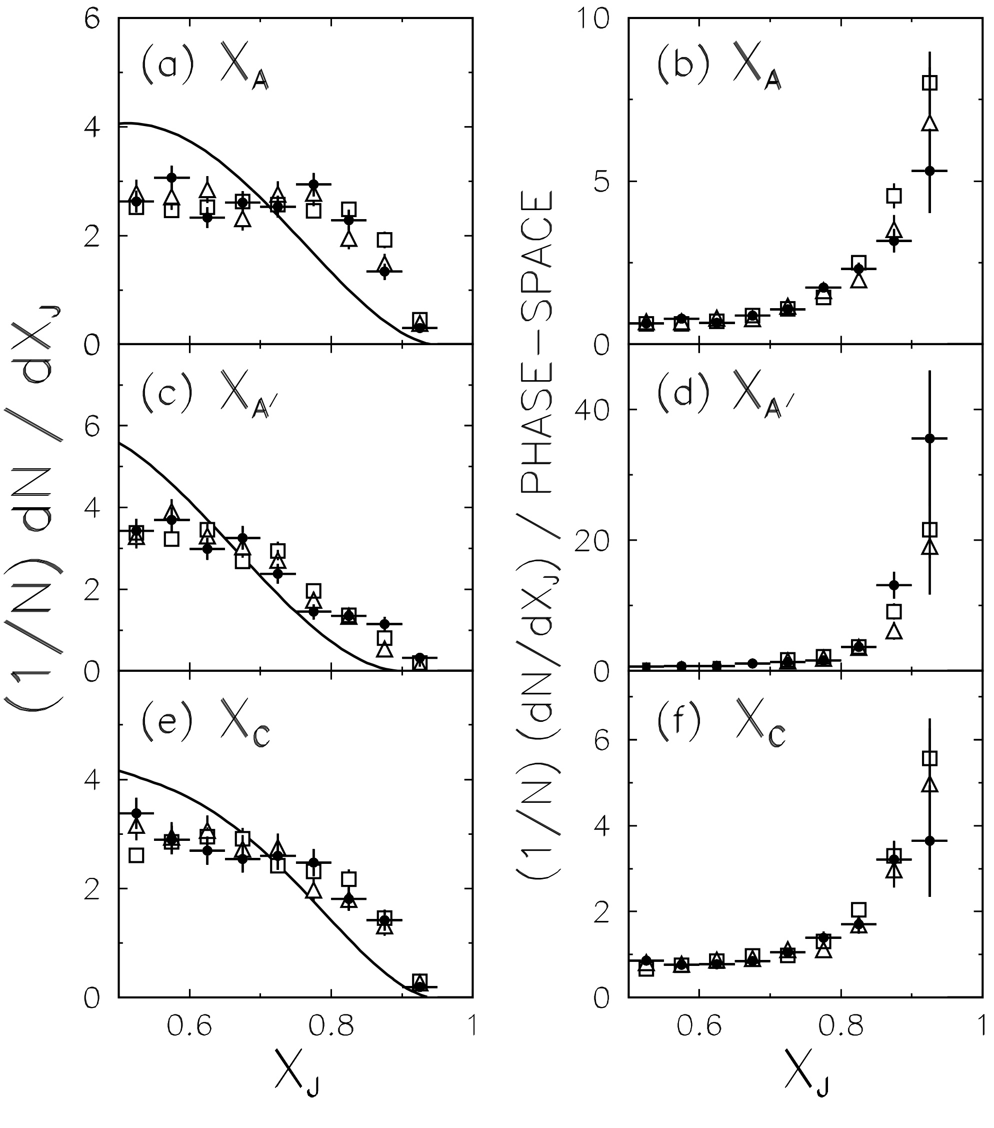

Figure 17: The two-body energy sharing distributions for inclusive four-jet and five-jet events. Data (points) are compared with HERWIG predictions (triangles), NJETS predictions (squares), and phase-space predictions (curves) for (a) X_A, (b) X_A after dividing by the phase-space model predictions, (c) $X_{A'}$, (d) $X_{A'}$ after dividing by the phase-space model predictions, (e) X_C, and (f) X_C after dividing by the phase-space model predictions.

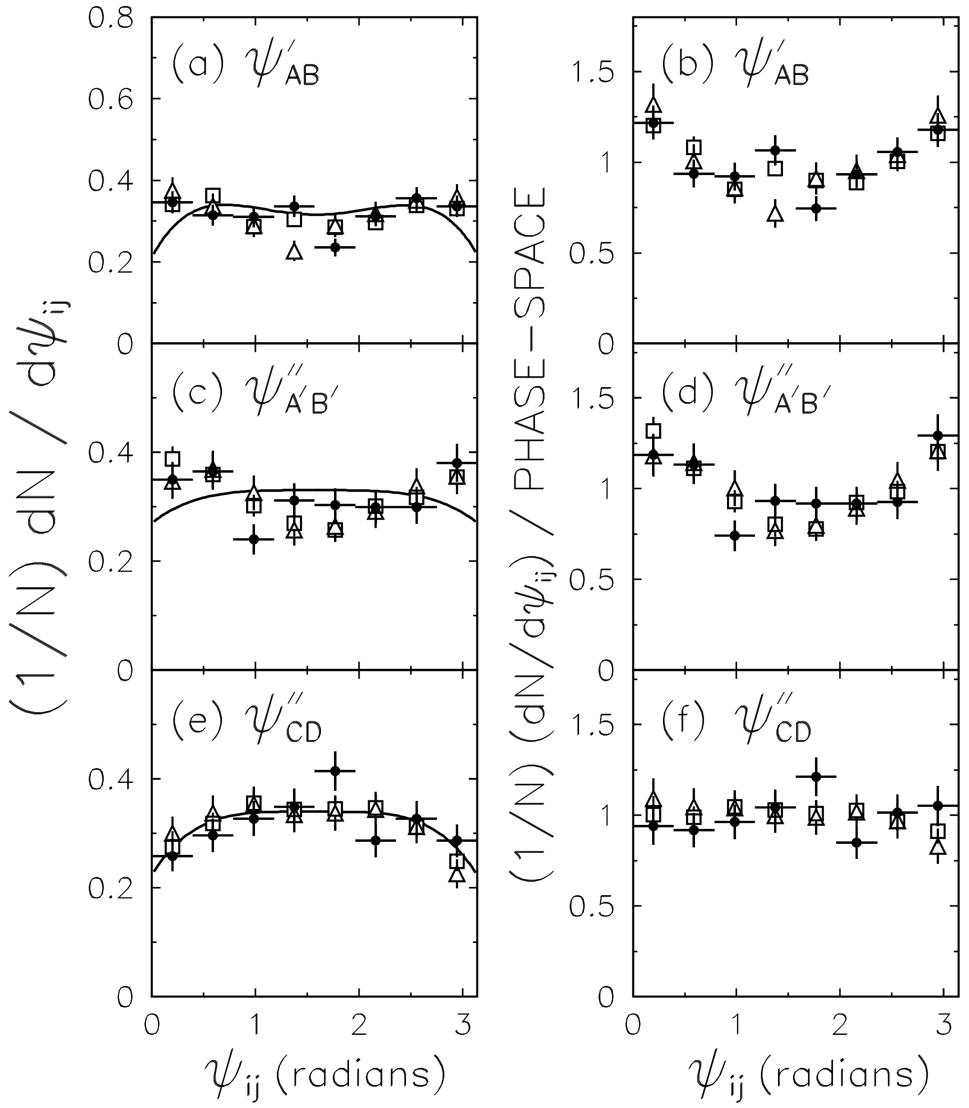

Figure 18: Two-body angular distributions for inclusive four-jet and five-jet events. Data (points) are compared with HERWIG predictions (triangles), NJETS predictions (squares), and phase-space predictions (curves) for (a) ψ'_{AB}, (b) ψ'_{AB} after dividing by the phase-space model predictions, (c) $\psi''_{A'B'}$, (d) $\psi''_{A'B'}$ after dividing by the phase-space model predictions, (e) ψ''_{CD}, and (f) ψ''_{CD} after dividing by the phase-space model predictions.

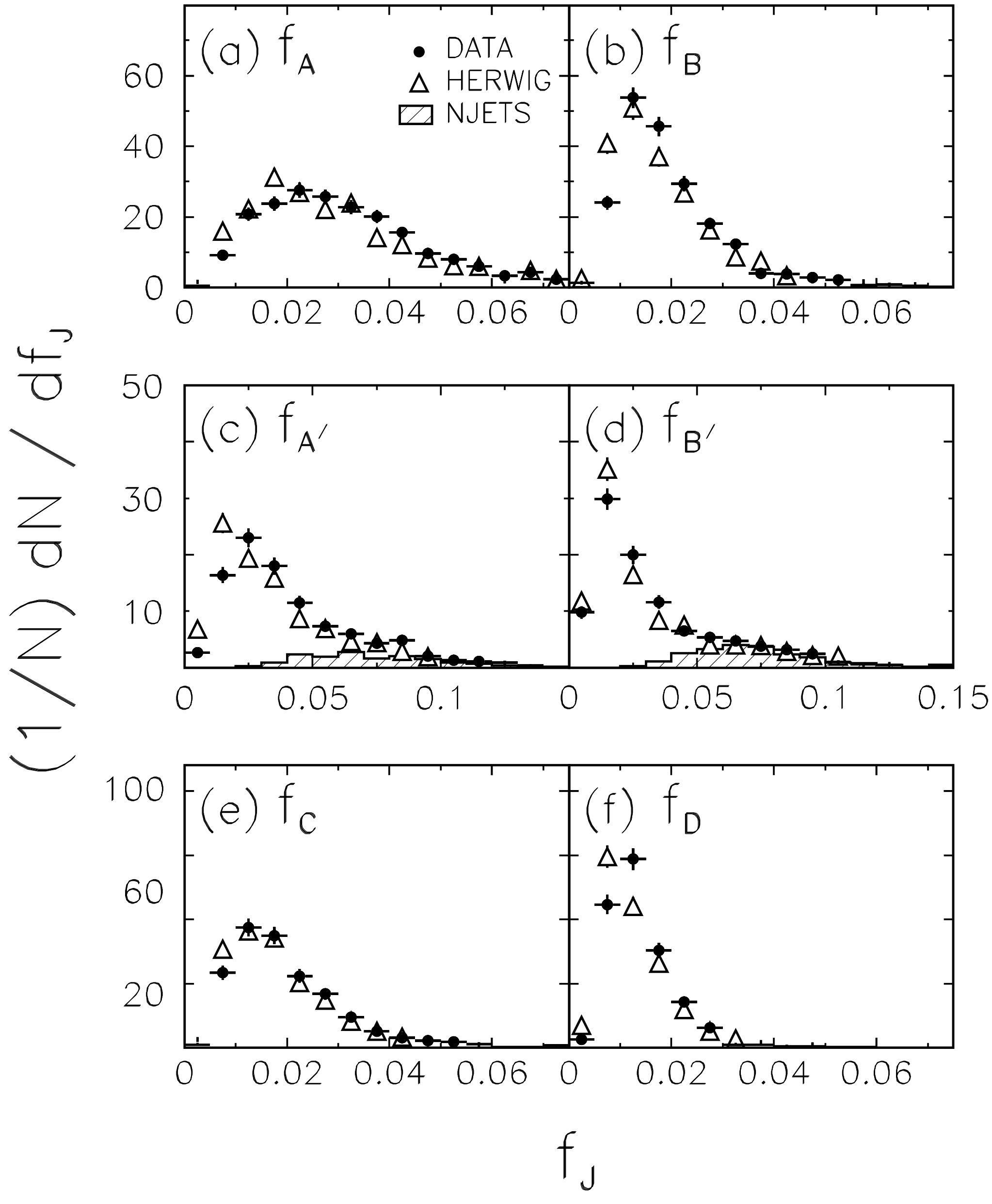

Figure 19: Single-body mass fraction distributions for two-body systems in inclusive four-jet and five-jet events. Data (points) are compared with HERWIG predictions (triangles), and NJETS predictions (histograms) for (a) f_A, (b) f_B, (c) $f_{A'}$, (d) $f_{B'}$, (e) f_C, and (f) f_D.